

## Research paper

A peptide derived from the core  $\beta$ -sheet region of TIRAP decoys TLR4 and reduces inflammatory and autoimmune symptoms in murine models

Asma Achek<sup>a</sup>, Hyuk-Kwon Kwon<sup>b</sup>, Mahesh Chandra Patra<sup>a</sup>, Masaud Shah<sup>a</sup>, Riwon Hong<sup>c</sup>, Wang Hee Lee<sup>a</sup>, Wook-Young Baek<sup>d</sup>, Yang Seon Choi<sup>a</sup>, Gi-Young Kim<sup>a</sup>, Thuong L.H. Pham<sup>a</sup>, Chang-Hee Suh<sup>d</sup>, Wook Kim<sup>a</sup>, Dae-Hyun Hahm<sup>c</sup>, Sangdun Choi<sup>a,\*</sup>

<sup>a</sup> Department of Molecular Science and Technology, Ajou University, Suwon 16499, Republic of Korea

<sup>b</sup> Department of Orthopaedics and Rehabilitation, Yale School of Medicine, New Haven, CT 06510, USA

<sup>c</sup> Department of Physiology, School of Medicine, Kyung Hee University, Seoul 02447, Republic of Korea

<sup>d</sup> Department of Rheumatology, Ajou University School of Medicine, Suwon 16499, Republic of Korea

## ARTICLE INFO

## Article History:

Received 3 May 2019

Revised 8 January 2020

Accepted 15 January 2020

Available online xxx

## Keywords:

Antagonist

TLR4

Collagen-induced arthritis

Systemic lupus erythematosus

Psoriasis

Decoy peptide

## ABSTRACT

**Background:** TLRs are some of the actively pursued drug-targets in immune disorders. Owing to a recent surge in the cognizance of TLR structural biology and signalling pathways, numerous therapeutic modulators, ranging from low-molecular-weight organic compounds to polypeptides and nucleic acid agents have been developed.

**Methods:** A penetratin-conjugated small peptide (TIP3), derived from the core  $\beta$ -sheet of TIRAP, was evaluated *in vitro* by monitoring the TLR-mediated cytokine induction and quantifying the protein expression using western blot. The therapeutic potential of TIP3 was further evaluated in TLR-dependent *in vivo* disease models.

**Findings:** TIP3 blocks the TLR4-mediated cytokine production through both the MyD88- and TRIF-dependent pathways. A similar inhibitory-effect was exhibited for TLR3 but not on other TLRs. A profound therapeutic effect was observed *in vivo*, where TIP3 successfully alleviated the inflammatory response in mice model of collagen-induced arthritis and ameliorated the disease symptoms in psoriasis and SLE models.

**Interpretation:** Our data suggest that TIP3 may be a potential lead candidate for the development of effective therapeutics against TLR-mediated autoimmune disorders.

**Funding:** This work was supported by the National Research Foundation of Korea (NRF-2019M3A9A8065098, 2019M3D1A1078940 and 2019R1A6A1A11051471). The funders did not have any role in the design of the present study, data collection, data analysis, interpretation, or the writing of the manuscript.

© 2020 The Author(s). Published by Elsevier B.V. This is an open access article under the CC BY-NC-ND license. (<http://creativecommons.org/licenses/by-nc-nd/4.0/>)

## 1. Introduction

Toll-like receptors (TLRs) are membrane-bound pattern recognition receptors that recognise exogenous pathogen-associated molecular patterns and/or endogenous damage-associated molecular patterns. Upon the detection of these patterns, TLRs trigger a dimerisation-driven complex signalling cascade that culminates in the activation of nuclear factor kappa light-chain enhancer of activated B cells (NF- $\kappa$ B) or interferon-regulatory factors (IRFs) [1,2]. After activation, these transcription factors spontaneously relocate into the nucleus and participate in the expression of proinflammatory cytokines [interleukin-1 (IL-1), IL-6, IL-1 $\beta$ , and IL-10], tumour necrosis factor  $\alpha$  (TNF- $\alpha$ ), and type I interferons (IFNs) [3].

All activated TLRs, except TLR3, recruit the adaptor protein (myeloid differentiation primary response 88; MyD88) through a bridging adaptor called Toll/IL-1 receptor (TIR) domain-containing adaptor protein (TIRAP). TLR3 recruits TIR domain-containing adaptor-inducing interferon  $\beta$  (TRIF) with the help of a bridging adaptor, TIR domain-containing-adaptor molecule (TRAM) [4]. In the MyD88-dependent pathway, recruitment of IL-1 receptor-associated kinase 4 (IRAK4) followed by IRAK1 or IRAK2 completes the formation of a supramolecular assembly called the myddosome [5,6], which is essential for subsequent signal transduction events. TLR4 is unique among all TLRs because it can also trigger the TRIF-dependent signal transduction, thereby complementing the TLR3-mediated induction of IFNs. Therefore, the overactivation of TLR4 in pathological conditions produces a significant amount of (pro)inflammatory molecules including chemokines, interferons, and interleukins that lead to an event termed a

\* Corresponding author.

E-mail address: [sangdunchoi@ajou.ac.kr](mailto:sangdunchoi@ajou.ac.kr) (S. Choi).

## Research in context

### Evidence before this study

A dysregulated response of Toll-like receptors (TLRs) is a hallmark of various inflammatory and autoimmune diseases; for this reason, the negative regulation of TLRs in pathological conditions has been investigated as a potential therapeutic strategy against the above-mentioned diseases. At present, several therapeutic modulators are being actively developed.

### Added value of this study

In this work, we report a penetratin-conjugated small peptide, TIP3, which blocks the TLR4-mediated inflammatory response *in vitro* and exerts a significant therapeutic effect *in vivo* by alleviating the inflammatory response in a mouse model of collagen-induced arthritis CIA and by relieving disease symptoms in murine models of systemic lupus erythematosus and psoriasis.

### Implications of all the available evidence

This study suggests that TIP3 halts the progression of rheumatoid arthritis, psoriasis, and systemic lupus erythematosus and ameliorates their symptoms by reducing the inflammatory response mediated by TLR signalling. Accordingly, this peptide may be a lead compound for the development of new therapeutics for inflammatory and autoimmune diseases.

previously unknown alternate adaptor-binding locations and homodimerisation interfaces have been proposed too [31]. Besides, a peptide derived from the BB loop segment of the TIR domain containing adaptor protein (TIRAP) was shown to block TLR2- and TLR4-mediated autoimmune responses [28].

TIRAP is a unique adaptor that acts as a bridge between activated TLRs (TLR2 and TLR4) and MyD88 during signal transduction [33]. TIRAP is constitutively associated with the cytoplasmic membrane through the phosphatidylinositol 4,5-bisphosphate–binding domain [34]. Nonetheless, the TIR domain of TIRAP is solvent exposed, facilitating the recruitment of MyD88 to the TIR domain of TLR2 or TLR4 [35–37]. The essential role of TIRAP in the downstream signalling of TLR2 and -TLR4 has been confirmed previously [36–38].

Herein, we found that a peptide derived from the first  $\beta$ -sheet ( $\beta$ A) of TIRAP, when conjugated with a cell-penetrating peptide (CPP; called penetratin), successfully inhibited agonist-induced TLR signalling. Remarkably, this peptide was effective against TLR3 and TLR4 signalling but did not exert a similar effect on other TLRs. In addition, we observed that TIP3 relieves the inflammatory response in a mouse model of collagen-induced arthritis (CIA), alleviates psoriasis symptoms in mice, and ameliorates the autoimmune response observed in a mouse model of systemic lupus erythematosus (SLE). Thus, TIP3 may turn out to be a promising therapeutic agent against inflammatory and autoimmune diseases.

## 2. Materials and methods

### 2.1. Reagents and cell line optimisation

RAW264.7 cells (macrophages; Korean Cell Line Bank, Seoul, Korea) were cultured in low-glucose Dulbecco's modified Eagle's medium (DMEM) containing 1% of a penicillin/streptomycin solution and 10% of foetal bovine serum (FBS) (Thermo Fisher Scientific, Inc., Waltham, MA, USA). HEK-Blue<sup>TM</sup> hTLR4 cells (InvivoGen, San Diego, CA, USA) were cultured in high-glucose DMEM containing 1% of the penicillin/streptomycin solution, 10% of FBS, and 0.2% of normocin. Human peripheral blood mononuclear cells (hPBMCs) and human mononuclear cells (hMNCs) were purchased from Lonza Inc. (Allendale, NJ, USA) and cultured in RPMI 1640 containing 2.05 mM L-glutamine, 1% of the penicillin/streptomycin solution, and 10% of FBS. THP-1 cells (kindly gifted by Dr. Chang-Hee Suh, Ajou University, Medical Centre, Suwon, Korea) were cultured in the RPMI 1640 medium supplemented with 1% of the penicillin/streptomycin solution and 10% of FBS and differentiated into macrophages using 80 nM phorbol 12-myristate 13-acetate (PMA; Sigma-Aldrich Co., St. Louis, MO, USA) for 24 h. All the cells were incubated in a humidified atmosphere containing 5% of CO<sub>2</sub> at 37 °C (Thermo Fisher Scientific, Inc.) and the media were refreshed after 18 h of incubation. PAM<sub>3</sub>CSK<sub>4</sub>, poly(I:C), R848 (resiquimod), and CpG-ODN were purchased from Thermo Fisher Scientific, Inc., FSL-1 from InvivoGen (San Diego, CA, USA), and lipopolysaccharide (LPS; *Escherichia coli* 0111:B4) from Sigma-Aldrich. All the peptides used in the experiments were synthesized by Peptron, Inc. (Daejeon, Korea) and BioStem (Ansan, Korea).

### 2.2. Mouse bone marrow-derived macrophages (mBMDM) culture optimisation

Six- to 7-week-old C57BL/6 J mice (RAONBIO, Seoul, Korea), maintained under pathogen-free conditions for 6–7 weeks, were used for the extraction of cells. Under aseptic conditions, the femurs and tibiae were collected from euthanised mice. Bone ends were separated, and the marrow cavities were flushed out with DMEM by means of a sterile 26-gauge needle. The suspended cells were incubated at 37 °C and 5% CO<sub>2</sub> for 1 h in a complete medium (DMEM, 10% FBS, 100 U/ml penicillin, and 100 µg/ml streptomycin; Thermo Fisher Scientific, Inc.). Next, the marrow cells were cultured with macrophage colony-

cytokine storm, which can result in a lethal autoinflammatory condition called sepsis.

The activation of innate immunity is predominantly protective because the secreted cytokines activate the B- and T-cell components of the adaptive immune system to combat infections [7].

Nonetheless, overactivation or dysregulation of this system is often detrimental for host survival. Autoantibodies expressed in response to self-antigens cause the onset of several autoimmune diseases, such as systemic lupus erythematosus (SLE) [8], rheumatoid arthritis (RA) [9], psoriatic arthritis [10], atherosclerosis [11], sepsis [12], and cancer and some other inflammatory diseases [13–15].

TLR3 and TLR4 have been implicated in the development and progression of several arthritic conditions, such as osteoarthritis, causing inflammation-associated destruction of bone tissues [16–18]. TLR4 has also been linked with neuroinflammatory disorders, such as Alzheimer's and Parkinson's disease, owing to its key role in the activation of the NOD-, LRR- and pyrin domain-containing protein 3 (NLRP3)-inflammasome [19]. In some studies, a significantly higher level of TLR3 has been observed in the serum samples of RA patients as compared to healthy individuals [20,21]. Moreover, the up-regulation of TLR4 in a murine model of lupus-like renal disease negatively affects the immune tolerance [22].

Using an experimental model of autoimmune encephalomyelitis, Reynolds et al. have found that the loss of TLR4 in CD4<sup>+</sup> T cells blunted the T helper-17 (Th-17) and Th-1 responses and abrogated the disease symptoms [23]. Therefore, the dysregulated TLRs are perceived as potent drug-targets for the treatment of autoinflammatory disorders and malignant diseases using a wide-range of therapeutic modulators [24–27].

In recent years, we witnessed exponential advances in peptide-based preclinical agents that inhibit cell surface-expressed TLRs (TLR2 [28] and TLR4 [29–31]) by targeting not only their extracellular domains but also their TIR domains [32]. The use of such peptides derived from protein–protein interaction surfaces has proven helpful in terms of identifying and validating interfaces that are indispensable for both partners. By means of the decoy peptide approach,

stimulating factor (M-CSF, 25 ng/ml; R&D Systems Inc., Minneapolis, MN, USA) and were harvested after 3–4 days. mBMDMs were isolated with Trypsin-EDTA and plated in a 60 mm dish. The TIP3-related experiments were conducted after 24 h.

### 2.3. Cell viability assay

The cell viability was measured using a colourimetric 1-(4,5-dimethylthiazol-2-yl)-3,5-diphenylformazan (MTT) assay (Sigma-Aldrich), which was carried out as described previously [39]. HEK-Blue<sup>TM</sup> hTLR4 cells were seeded at a density of  $5 \times 10^4$ /well, and RAW264.7 and THP-1 cells were seeded at  $2 \times 10^5$ /well. All the cells were grown overnight in 96-well plates (BD Biosciences, San Jose, CA, USA).

### 2.4. The secreted alkaline phosphatase (SEAP) activity assay

HEK-Blue<sup>TM</sup> hTLR4 cells were seeded at density  $2 \times 10^5$ /well and grown overnight in 24-well plates (BD Biosciences). The cells were treated with different concentrations of TIP3 in the presence and/or absence of LPS. Aliquots of supernatants (200 µl) from the treated cells were transferred to microcentrifuge tubes and heated for 10 min at 65 °C on a heating block (FINEPCR Co., Seoul, Korea). Supernatants were later placed in new 96-well plates (BD Biosciences), and SEAP production was detected with the HEK-Blue<sup>TM</sup> detection kit (InvivoGen, San Diego, CA, USA). Absorbance was measured on a microplate reader (Molecular Devices Inc., Silicon Valley, CA, USA) at 620 nm.

### 2.5. Western blot analyses

Total-protein extraction was performed using the M-PER mammalian protein extraction reagent (Thermo Fisher Scientific, Inc.). The concentration of proteins was measured with the bicinchoninic acid (BCA) assay kit (Sigma-Aldrich). Western blot analysis, including gel electrophoresis and transfer, was conducted using the Mini-PROTEAN Tetra Cell and mini trans-blot electrophoretic transfer cell system (Bio-Rad Laboratories, Hercules, CA, USA) [39]. The membranes were immunoblotted with specific primary antibodies (1:500–1000) against phosphorylated (p)-p65, JNK, p-JNK, p-IRF3, p-ERK, ERK, p-p38, p38, and Iκ-Bα (Cell Signalling Technology Inc., Danvers, MA, USA); p-ERK, p-p38, JNK, ATF3, COX2, and β-actin (Santa Cruz Biotechnology Inc., Dallas, TX, USA); and iNOS (BD Biosciences) with gentle shaking at 4 °C overnight. After that, the membranes were rigorously washed with phosphate-buffered saline (PBS) containing 0.1% of Tween 20 (PBST) and incubated with a peroxidase-conjugated anti-mouse or anti-rabbit IgG antibody (1:1000) for 2 h. The proteins were detected by means of a SuperSignal West Pico ECL solution (Thermo Fisher Scientific, Inc.) and visualised on a ChemiDoc<sup>TM</sup> Touch Imaging System (Bio-Rad Laboratories).

### 2.6. Confocal microscopy

RAW264.7 cells were seeded at a density of  $2 \times 10^5$ /well in 24-well plates (BD Biosciences) containing coverslips and were grown overnight. The cells were treated with TIP3 (50 µM) for 1 h before LPS stimulation (100 ng/ml). After that, the cells were fixed in a 3.7% formaldehyde solution (Sigma-Aldrich) and permeabilised with a 0.2% Triton X-100 solution (AMRESCO, Solon, OH, USA) for 15 min. The cells were then washed with PBS and blocked with 2% bovine serum albumin (BSA) solution (Thermo Fisher Scientific, Inc.). These cells were then incubated with the anti-p-p65 antibody (1:1000; Santa Cruz Biotechnology Inc.) for 2 h and rigorously washed with PBS. Next, the cells were incubated with an Alexa Fluor 546-conjugated secondary antibody (Invitrogen, Carlsbad, CA, USA) for 1 h and were washed with PBS three times. A Hoechst 33258 solution (5 µM;

Sigma-Aldrich) was employed to stain nuclei. Fluorescence intensities were measured by confocal microscopy (LSM-700; Carl Zeiss Microscopy GmbH, Munich, Germany), and images were analysed in the Zen 2009 software.

### 2.7. TNF-α, IL-6, and IFN-β cytokine detection assays

RAW264.7 cells, hMNCs, mBMDMs, and THP-1-derived macrophages were seeded at density  $2 \times 10^5$ /well in 96-well plates (BD Biosciences) or  $5 \times 10^5$ /well in 24-well plates (BD Biosciences) and grown overnight. After 24 h of treatment, IFN-β secretion was measured by means of the LEGEND MAX<sup>TM</sup> Mouse IFN-β pre-coated Enzyme-linked immunosorbent assay (ELISA) Kit (BioLegend, San Diego, CA, USA). The IL-6 secretion was assessed with the Mouse IL-6 ELISA MAX<sup>TM</sup> Deluxe Kit (BioLegend) or Mouse IL-6 Platinum ELISA Kit (eBioscience, San Diego, CA, USA), and TNF-α production was assessed using the Mouse TNF alpha ELISA Ready-SET-Go!® Kit (eBioscience). hMNCs were seeded at a density of  $2 \times 10^5$ /well in 96-well plates (BD Biosciences) and grown overnight. After 24 h of TIP3 treatment, the secretion levels of IL-6 and TNF-α were assessed with Human IL-6 and TNF alpha ELISA MAX<sup>TM</sup> Deluxe (BioLegend) kits, respectively. The plates were then analysed on a microplate spectrophotometer system (Molecular Devices) at the respective wavelengths.

### 2.8. Quantification of intracellular nitric oxide (NO) and reactive oxygen species (ROS) and NO secretion assay

RAW264.7 cells were seeded at  $1 \times 10^6$  in 6 cm culture dishes (SPL Life Sciences, Pochun, Korea) and grown overnight. After LPS stimulation and TIP3 treatment, intracellular NO and ROS were quantified by means of DAF-FM and DCF-DA dyes (Thermo Fisher Scientific, Inc.) as described elsewhere [40]. Fluorescence intensity of the cells was analysed on a FACSaria III instrument with the Diva software (BD Biosciences). For the assessment of production of extracellular NO, RAW264.7 cells and mBMDMs were seeded at a density of  $2 \times 10^5$ /well and grown overnight in 96-well plates (BD Biosciences). Secretion of NO was measured with the Nitric Oxide Detection Kit (iNtRON Biotechnology Inc., Seongnam, Korea) [39]. The absorbance was read on a microplate spectrophotometer system (Molecular Devices) at 550 nm.

### 2.9. Quantitative RT-PCR analysis

RAW264.7 cells and THP-1 cells were treated with TIP3 (50 µM) for 1 h before LPS stimulation (100 ng/ml) for 3 or 4 h, respectively. Total RNA was isolated from the cells using the TRIzol® Reagent (Invitrogen). Total RNA concentration was measured on a micro UV–Vis fluorescence spectrophotometer (e-spect, Malcom, Japan), and cDNA was synthesized using the iScript<sup>TM</sup> cDNA Synthesis Kit (Bio-Rad Inc.). Quantitative RT-PCR was carried out with the Light Cycler® 480 SYBER Green I Master kit (Roche Life-science Inc.) and pre-designed primers specific for genes Il-1β, Il-6, Il-8, Tnf-α, Inf-β, Cxcl-10, β-actin, and Gapdh (Bionics, Seoul, Korea; Supp Table 1). Gene expression levels were measured using a Real-Time PCR detection system (Qiagen, Hilden, Germany) by the SYBR Green technique and the data were analysed by the ΔΔC<sub>t</sub> method.

### 2.10. Preparation of diseases mouse models

#### 2.10.1. RA model preparation and TIP3 treatment

Male DBA/1 J mice weighing 20–23 g (6 to 7 weeks old) were purchased from Central Lab Animal Inc. (Seoul, Korea). The mice were housed in a limited-access rodent facility at up to four animals per polycarbonate cage on a 12 h light/dark cycle (at 22–24 °C) with free access to pelleted food and water. CIA was induced according to the

previously described protocol [41]. Briefly, the mice were immunised at the base of their tails with a mixture of 100 µg of chicken type II collagen (CII, Sigma-Aldrich) and an equal volume of complete Freund's adjuvant solution (Sigma-Aldrich); this time point was designated as day 0. The mice were then given a booster (second) injection of the mixture on day 20.

All the mice were randomly subdivided into six experimental groups each containing seven animals ( $n = 7$ ). The groups were designated as follows: (1) untreated normal group (Normal); (2) the vehicle-treated arthritis group (CIA); the TIP3-treated arthritis groups subdivided into (3) the 2.5 nmol/g TIP3-treated group (named CIA-TIP3-2.5), and (4) the 10 nmol/g TIP3-treated group named CIA-TIP3-10; (5) the postarthritis phase (PAP)-TIP3-10 group (10 nmol/g TIP3-injected mice at PAP); and (6) the methotrexate (MTX)-treated arthritis group named MTX (2 mg/kg). TIP3 or methotrexate dissolved in saline was intraperitoneally (i.p.) injected once a day, starting on day 22.

To evaluate arthritis progression in the CIA mice, body weight, paw volume, and the arthritis index were determined. The mouse body weights were measured using a digital balance (Mettler-Toledo Inc., Columbus, OH, USA). Joint pain in the hind limb was evaluated by the squeaking score during forced flexion and extension of the ankle joint, 10 times every 5 s. A score of 0 (no vocalisation) or 1 (vocalisation) was given to each hind limb for every flexion and extension procedure. Total numbers of vocalisations detected by the observer were then calculated as the squeaking score. Paw volume was measured by the volume displacement of an electrolyte solution in a water-displacement plethysmometer (Ugo-Basil Biological Research Apparatus Co., Comerio-Varese, Italy) as described elsewhere [42,43]. Paw volume was expressed as a relative value compared with that on day 0, which was defined as 1.0 (100%). The arthritis index was assessed by grading the apparent arthritic severity of all joints of the limbs on a four-point scale per mouse: 0 = no erythema or swelling of any joint in one limb, 1 = erythema or swelling of at least one joint per limb, 2 = erythema or swelling of fewer than three joints per limb, 3 = erythema or swelling of all joints in one limb, and 4 = ankylosis and deformity of all joints in one limb. The maximal score was 16 for each mouse. The behavioural tests were performed twice a week on each animal.

For imaging, bone samples were fixed with a 10% formalin solution to prepare them for micro-computed tomography (micro-CT). Bone specimens were scanned in the knee joint using an *In-vivo* Micro-CT device (NFR Polaris-G90; NanoFocus Ray Co., JeonJu, Korea). The following settings were employed: an X-ray voltage of 55 kV, X-ray current of 105 µA, X-ray spot size of 8 µm, and exposure time of 80 ms for each of the 180° rotational steps. Reconstruction of 3D images of the knee joints and 2D images of the trabecular bone (in the sagittal section at the top of the tibia) and of the cortical bone (in the horizontal section in the middle of the tibia) was performed in Data viewer, CTvox, and CTAn software packages (SkyScan, Kontich, Belgium) on 500 slices. The bone mineral density of each reconstructed knee joint was measured at 1 mm from the top of the tibia after setting the region of interest.

#### 2.10.2. The mouse model of psoriasis and the TIP3 treatment procedure

The 6–7 weeks old C57BL/6 mice, were purchased from orient Bio Inc. (Seongnam, South Korea), housed under specific pathogen-free conditions, and provided with standard laboratory diet (STD) *ad libitum*. Psoriasis-like symptoms were generated by topical application of 62.5 mg of Aldara cream (5%) (Aldara; 3 M Pharmaceutical LLC.), which contains imiquimod (IMQ), for 5 consecutive days. IMQ was not applied in the control group. Mice were administered with daily doses of TIP3 (10 or 50 nmol/g) or PBS as a control, 1 day before the application of the Aldara cream (5%). MTX (10 µg/g; cat. # M9929, Sigma-Aldrich) was also administered as the positive control, 1 day before application of the IMQ cream. After 5 days, the mice were

euthanised under respiratory anaesthesia, and skin lesions, the spleen, and serum samples were collected for analysis. To score the inflammation severity of back skin, an objective scoring system was developed based on the clinical Psoriasis Area and Severity Index (PASI). Erythema, scaling, wrinkles, and thickening were scored independently from 0 to 4 as follows: 0, none; 1, slight; 2, moderate; 3, substantial; and 4, very well pronounced. Erythema, scaling, and thickness were scored under careful supervision of experienced researchers. The cumulative score (erythema plus scaling plus thickening, scale 0–12) indicated the severity of the psoriasis symptoms.

#### 2.10.3. The lupus model and TIP3 treatment

Three female wild-type (C57BL/6) and lupus-prone mice (MRL/lpr), each initially weighing 18–20 and 38–40 g, respectively, were purchased from Jackson Laboratory (Bar harbor, ME, USA). The mice were allowed to acclimate for 1 week and were bred under pathogen-free conditions according to the approved guidelines of Ajou University School of Medicine. The mice in the vehicle group were i.p. injected with 1% dimethyl sulfoxide (DMSO), while others with TIP3 at a dose of 10 nmol/g per day (dissolved in 1% DMSO) for 20 days, and their weight was monitored daily. The mice were euthanised at the end of experiments, and their blood, urine, and tissues were collected. After 1 h incubation, blood samples were collected into serum separation tubes, centrifuged at 3000 rpm for 10 min at 20 °C, and stored at –80 °C. The collected urine samples were immediately stored at –80 °C, whereas the tissue samples were thoroughly washed with PBS and immersed in the RNA stabilisation solution (Qiagen Sciences, Maryland, MD, USA). The concentrations of anti-double-stranded DNA (dsDNA) antibodies, and of C3 complement were analysed by ELISA. Besides, mouse urinary albumin levels were determined with the Mouse Albumin ELISA Kit (41-ALBMS-E01, Alpco Diagnostics, Salem, NH, USA). Three independent measurements were performed per sample.

#### 2.11. Histological analysis & immunochemical staining

Skin samples from the back lesions of mice were fixed in a 4% paraformaldehyde solution, embedded in paraffin, and sectioned at 7 µm thickness onto glass slides. The sections were stained with hematoxylin and eosin (H&E) to evaluate the thickness of the epidermis and dermis. The thickness of skin was measured under a Leica DMi8 fluorescence microscope using Leica LAS X Hardware Configurator. IMQ-induced inflammation in the skin was evaluated using the mouse-specific HRC/DAB Detection IHC Kit (Abcam, cat. # AB64259) using primary antibodies recognizing CD68, CD4, and IL-17.

#### 2.12. Evaluation of TLR-binding kinetics of TIP3 by the Surface Plasmon Resonance (SPR) assay and in silico analyses

SPR experiments were conducted on a Reichert 4SPR machine (Reichert Technologies Depew, New York, USA) using the Planar Polyethylene Glycol/Carboxyl (PEG) Sensor Chip. PBST containing 2% of DMSO served as running buffer and 50 mM HCl solution was used for regeneration. The TIR domains of TLR3 and TLR4, synthesized by Bioneer (Daejeon, Korea), were immobilised onto the surfaces of the sensor chip at a concentration of 30 µg/ml using 20 mM sodium acetate solutions at pH 5.5 and 5.0, respectively. Various concentrations of TIP3 ranging from 0 to 12.5 µM were injected into the chip to evaluate the binding of TIP3 to the immobilised proteins; running buffer was injected into the empty channel as a reference. The experiments were conducted in duplicate with freshly prepared reagents. The Reichert 4SPR evaluation software was utilised to analyse the data. Detailed methods related to the *in silico* analyses are provided in the supplementary methods.

## 2.14. Statistical analysis

All data analyses were performed by the *t*-test in SigmaPlot software (12.0 version, Systat Software Inc., San Jose, CA, USA) or GraphPad Prism 5 (GraphPad Software, Inc., CA, USA). All experiments were conducted independently for at least three times and the statistical significance was defined as a P-value of \*  $P < 0.05$ , \*\* $P < 0.01$ .

## 2.15. Ethics approval

All animal care and experimental procedures for the RA model were conducted in accordance with the NIH Guide for the Care and Use of Laboratory Animals protocol and were approved by the Institutional Animal Care and Use Committee (IACUC) of Kyung-Hee University [Permit number: KHUASP(SE)-15-115]. As of the psoriasis and lupus, the animal experiments were approved by the IACUC at Ajou University (approval No. 2017-0002 for the psoriasis model and approval No. 2017-0022 for the lupus model).

## 3. Results

### 3.1. Selection and validation of the TIRAP-derived TLR-inhibitory peptides

The protein-protein interface has been widely exploited by manipulating the interface knowledge to disrupt a particular signalling pathway. We had recently explored two peptides [TIP1 ( $\beta$ C strand) and TIP2 ( $\beta$ D strand)] from the central region of the TIRAP TIR domain and found that TIP1, but not TIP2, abrogates multiple TLR signalling pathways by interfering with the adaptor recruitment process [44]. The present study describes the TLR-inhibitory property of a third peptide (TIP3) that is derived from the first  $\beta$ -strand ( $\beta$ A) of the TIRAP core (Fig. 1a, b). TIP2 (serving as the negative control) and TIP3 were commercially synthesised and conjugated with the CPP, isolated from the Drosophila antennapedia homeodomain (KKWKMRRNQFWIKIQR) [45], for the efficient intracellular delivery. Both peptides did not show any significant cytotoxicity at any of the concentrations tested, ranging from 12.5 to 50  $\mu$ M, but manifested slight cytotoxicity when evaluated at a high concentration, 100  $\mu$ M. Concentration-dependent viability data suggested that both peptides had no effect on cell viability at 50  $\mu$ M or below and were thus assumed safe within this range for further experiments (Fig. 1c). To study the inhibitory effects of the selected peptides, initially, we measured the NF- $\kappa$ B level in the SEAP activity assay based on HEK-Blue<sup>TM</sup> hTLR4 cells stimulated by LPS. The results showed that TIP3, but not TIP2, hampered the LPS-induced SEAP activity in a dose-dependent manner (Fig. 1d). To rule out the possibility that the CPP alone or/and unconjugated TIP3 (referred to as TIP3 w/o CPP) have any modulatory effect on the LPS-induced pathways, both peptides were synthesized (Peptron, Inc.) and evaluated for their effect on cell viability, LPS-induced TNF- $\alpha$  secretion, and protein expression. Both peptides did not affect the cell viability at  $\leq 50$   $\mu$ M and did not have any modulatory effect on TNF- $\alpha$  secretion. Furthermore, neither peptide inhibited  $I\kappa$ -B $\alpha$  degradation, phosphorylation of the p65 subunit of NF- $\kappa$ B (p-p65), or the expression of mitogen-activated protein kinase (MAPKs) in RAW264.7 cells (Supp Fig. 1a-c), suggesting that the CPP is simply an efficient carrier of the TIP3; without the CPP, TIP3 is unable to cross the cell membrane and reach its target. The specificity of TIP3 towards the TLR signalling pathway was further narrowed down by evaluating the TLR4- and TNFR-mediated inflammasome activation and IL-1 receptor (IL-1R) pathways. For the NLRP3 activation, THP-1 cells were primed with either LPS or a recombinant human TNF- $\alpha$  protein and subsequently activated with Nigericin for the induction of IL-1 $\beta$ . The data revealed that TIP3 dose-dependently inhibits IL-1 $\beta$  secretion in LPS-primed cells, but not in the TNF- $\alpha$ -primed cells (Supp Fig. 1d, e). Besides, TIP3 did not hinder the

secretion of IL-8 following the activation of THP-1 cells with IL-1 $\beta$  (Supp Fig. 1f) suggesting that the inhibitory impact of TIP3 is indeed specific to the TLR signalling pathway.

### 3.2. TIP3 inhibits MyD88-dependent and -independent TLR4 and TLR3 signalling in macrophages

Of all TLRs, only TLR4 can simultaneously activate the downstream signalling network through the adaptor proteins MyD88 and TRIF in a time-dependent manner [17,46,47]. Thus, we decided to examine the inhibitory effect of TIP3 on both signalling arms of the TLR4 pathway in LPS-stimulated murine RAW264.7 cells. TIP3 did not have any toxic effects on RAW264.7 cells at 50  $\mu$ M (Fig. 2a), thereby confirming the above-mentioned HEK-Blue<sup>TM</sup> hTLR4 viability results. The western blot data revealed that TIP3 suppressed LPS-induced MyD88-dependent as well as -independent signalling pathways by inhibiting  $I\kappa$ -B $\alpha$  degradation, and phosphorylation of the p65 subunit of NF- $\kappa$ B, and IRF3 (p-IRF3; Fig. 2b). Besides, TIP3 hindered the LPS-induced expression of activating transcription factor 3 (ATF3), and the expression of MAPKs by inhibiting the phosphorylation of c-Jun N-terminal kinase (JNK), p38 MAPK, extracellular signal-regulated kinase (ERK), and p38 in these cells (Fig. 2b and c). Confocal microscopy analysis confirmed that TIP3 decreased the LPS-induced p65 phosphorylation (Fig. 2d). In agreement with these findings, TIP3 significantly prevented *in vitro* production of proinflammatory cytokines (TNF- $\alpha$  and IL-6) and IFN- $\alpha$  and - $\beta$  in a dose-dependent manner (Fig. 2e-h).

The stimulation of TLR4 by its cognate ligands leads to the induction of cyclooxygenase 2 (COX2) and inducible nitric oxide synthase (iNOS) as well as the production of NO in RAW264.7 cells [25,48]. Moreover, it has been reported that stimulation of primary macrophages by LPS is responsible for the induction of both mitochondrial and intracellular formation of ROS [49,50]. Our data revealed that TIP3 successfully represses the LPS-induced extracellular secretion of NO and the expression of iNOS and COX2 in a dose-dependent manner (Fig. 2i and j). Similarly, the intracellular production of NO and ROS was significantly inhibited (Fig. 2k and l). Taken together, these findings suggested that TIP3 inhibits LPS-induced MyD88-dependent as well as -independent TLR4 signalling in RAW264.7 cells.

To assess the effects of TIP3 on other TLRs, the TNF- $\alpha$  secretion level was measured in RAW264.7 cells after treatment with various TLR ligands: PAM<sub>3</sub>CSK<sub>4</sub> (TLR1/2), FSL-1 (TLR2/6), Poly(I:C) (TLR3), resiquimod (TLR7/8), or CpG-ODN (TLR9). Of note, TIP3 yielded somewhat weak inhibition of TNF- $\alpha$  secretion mediated by TLR1/2, TLR2/6, TLR7, TLR8, and TLR9 at 50  $\mu$ M, but significantly diminished the TLR3-mediated TNF- $\alpha$  secretion in a dose-dependent manner (Fig. 2m and n). Similarly, poly(I:C)-induced secretion of IL-6, IFN- $\alpha$ , and IFN- $\beta$  was also inhibited in RAW264.7 cells (Fig. 2o and p). In line with the inhibition of protein expression levels, TIP3 significantly inhibited the mRNA expression of *Tnf- $\alpha$* , *Il-6*, *Ifn- $\beta$* , *Cxcl-10*, and *Il-1 $\beta$*  genes in murine macrophages as evidenced by quantitative RT-PCR (Fig. 2q-v).

### 3.3. The TLR4- and TLR3-inhibitory effects of TIP3 are reproducible in primary cell lines

To extend the evaluation of the inhibitory effects of TIP3, as observed in RAW264.7 cells, similar experiments were conducted on THP-1-derived macrophages. In the absence of any cytotoxicity (Fig. 3a), we assessed the effect of the peptide on LPS-induced activation of NF- $\kappa$ B and MAPKs by western blot analysis. The results indicated that TIP3 successfully hindered the activation of NF- $\kappa$ B and ATF3 and the phosphorylation of IRF3 in hPBMCs (Fig. 3b). TIP3 also inhibited the phosphorylation of MAPKs, including ERK, JNK, and p38 in these cells (Fig. 3c). Furthermore, TIP3 had a significant dose-dependent inhibitory effect on TNF- $\alpha$  and IL-6 secretion by THP-1

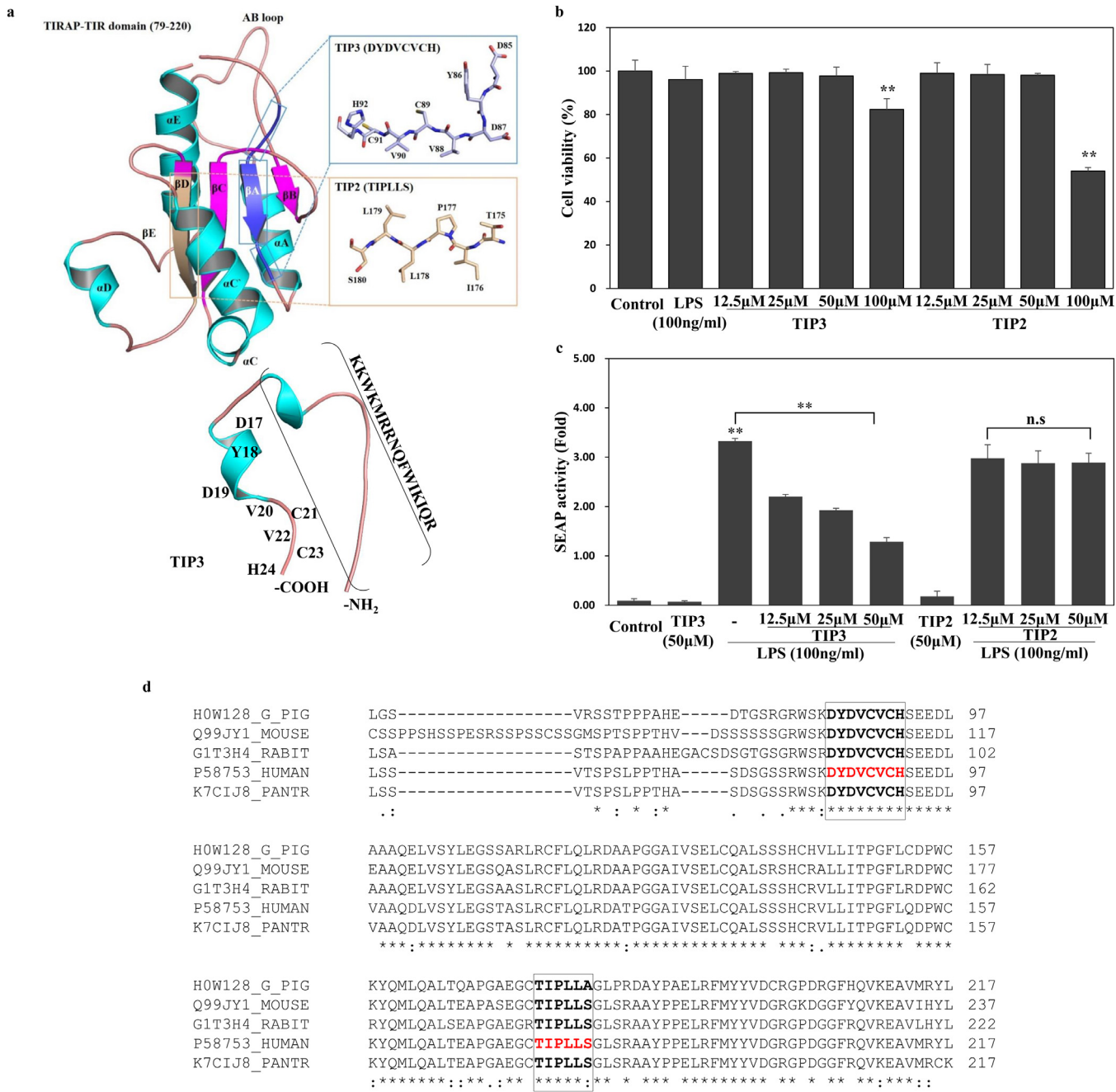


**Fig. 1.** Selection and initial evaluation of the TIRAP-derived TLR-inhibitory peptides. (a) The TLR-inhibitory peptide TIP3 (DYDVCVCH) was selected from the first  $\beta$ -strand  $\beta$ A (blue box). The peptide, TIP2 (TIPLLS), was taken from the  $\beta$ D and served as a negative control. Both peptides were N-terminally fused with a cell-penetrating peptide (CPP) derived from the Drosophila antennapedia homeodomain (KKWKMRNQFWIKIQR) to facilitate their intracellular delivery. (b) The cell viability assay suggests that TIP3 and TIP2 do not affect the cell viability at  $\leq 50 \mu\text{M}$ . (c) The substantial inhibition of NF- $\kappa$ B activation (measured by the SEAP assay) by TIP3 but not TIP2, was assumed to be the initial hallmark of the TLR-inhibitory capacity of TIP3. (d) Sequence alignment between TIRAP TIR domains from selected species. Only the portion of the alignment that covers TIP2 and TIP3 peptides is shown. The identical residues are indicated by ‘\*’, conservative substitutions and semiconservative substitutions are marked with ‘.’ and ‘:’, respectively. The data shown represent at least three independent experiments ( $n \geq 3$ ), and bars indicate means  $\pm$  SEM (\* $P < 0.05$ , \*\* $P < 0.01$ ) according to two-tailed Student’s *t*-test.

cells (Fig. 3d and e). The mRNA expression of proinflammatory cytokines (IL-6, TNF- $\alpha$ , and IL-1 $\beta$ ) and the chemokine (IL-8) was monitored in THP-1 cells after treatment with TIP3 (50  $\mu$ M) for 1 h followed by cotreatment with LPS for 4 h. Our data revealed that TIP3 successfully inhibited LPS-induced mRNA expression of these cytokines and of IL-8 (Fig. 3f-i).

Likewise, the inhibitory effect of TIP3 was evaluated on primary mBMDMs cells. The cells were pretreated with TIP3 for 1 h followed by cotreatment with LPS for 24 h. TIP3 suppressed the TLR4-mediated secretion of IL-6 and TNF- $\alpha$  (Fig. 3j, h), and the TLR3-mediated secretion of IFN- $\beta$  in mBMDMs (Fig. 3l). A significant reduction in the LPS-

induced extracellular generation of NO was observed too (Fig. 3m). When tested in hMNCs, TIP3 had similar potency, and substantial reproducible outcomes were observed in terms of cell viability (Fig. 3n) and cytokine inhibition. TIP3 significantly inhibited the TLR4-mediated IL-6 secretion and TLR4- and TLR3-mediated secretion of TNF- $\alpha$  (Fig. 3o-q).

### 3.4. TIP3 has a potent therapeutic effect in the CIA model

Numerous researchers have delineated the involvement of TLR4 in the inflammatory response associated with RA and osteoarthritis.

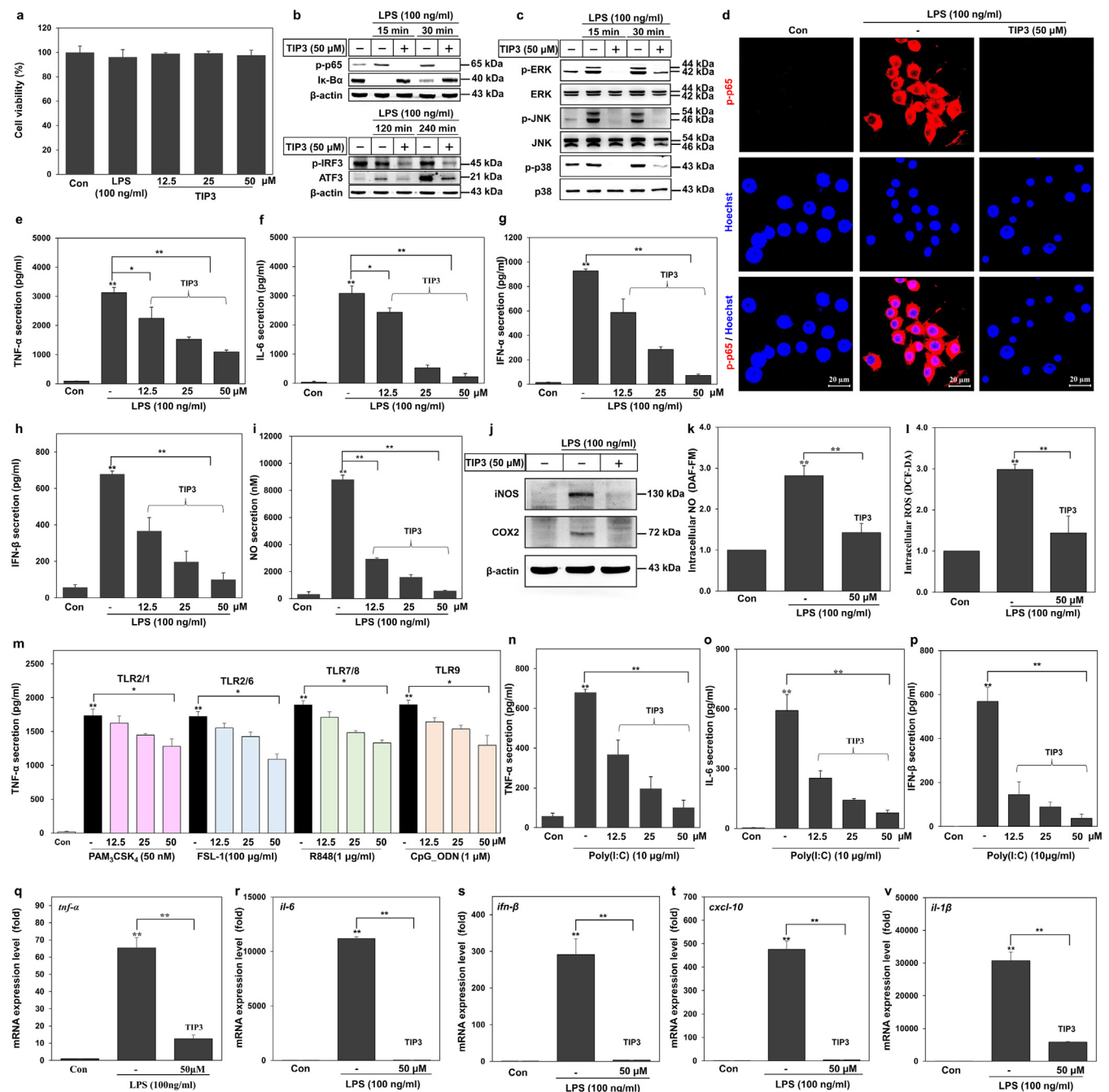


**Fig. 2.** TIP3 inhibits the signalling pathways of TLRs by downregulating the transcription factors and proinflammatory cytokines. (a) TIP3 was found to be safe at 50  $\mu$ M for RAW264.7 cells and other cell lines in the subsequent experiments. (b, c) The protein expression levels of p-p65, I $\kappa$ -B $\alpha$ , p-IRF3, ATF3, p-ERK, ERK, p-JNK, JNK, p-p38 and p38 were measured by western blotting of the total-protein extract, where  $\beta$ -actin served as a loading control. (d) Phosphorylation of NF- $\kappa$ B (p-p65) was evaluated by immunofluorescent staining and confocal microscopy. Hoechst was utilised for nucleus staining (the scale bar represents 20  $\mu$ m). (e–h) Secretion levels of TNF- $\alpha$ , IL-6, IFN- $\alpha$ , and IFN- $\beta$  were measured by ELISAs. The release of four cytokines was dose-dependently inhibited by TIP3. (i) The NO secretion level was evaluated using a standard NO secretion kit. (j) The expression levels of iNOS and COX2 were measured by western blotting;  $\beta$ -actin served as a loading control. (k, l) Intracellular NO and ROS were quantified by DAF-FM and DCF-DA staining, respectively, and were found to be substantially downregulated by 50  $\mu$ M TIP3. (m) Inhibitory effects of TIP3 on multiple TLRs were evaluated by measuring the TNF- $\alpha$  level, when cells were activated with PAM<sub>3</sub>CSK<sub>4</sub> (TLR2/1), FSL-1 (TLR2/6), R848 (TLR7/8), or CpG-ODN (TLR9) at various concentrations. These TLRs were not inhibited by TIP3 as significant as by TLR4. The TLR3-inhibitory effect of TIP3 was investigated through the secretion of (n) TNF- $\alpha$ , (o) IL-6, and (p) IFN- $\beta$  in RAW264.7 cells after their activation by poly(I:C) (TLR3) for 24 h. (q–v) Effects of TIP3 on the LPS-induced mRNA expression levels of *Tnf- $\alpha$* , *Il-6*, *Ifn- $\beta$* , *Cxcl-10*, and *Il-1 $\beta$*  after 3 h of treatment. Values are indicated as fold changes (relative quantification; RQ) in mRNA levels, normalized to  $\beta$ -actin. The data shown represent at least three independent experiments ( $n \geq 3$ ), and bars denote mean  $\pm$  SEM (\* $P < 0.05$ , \*\* $P < 0.01$ ) according to two-tailed Student's t-test.

with the hope of ascertaining new therapeutic strategies [9,17,51]. We also investigated the possible anti-inflammatory effect of TIP3 in chronic inflammatory diseases such as RA using a mouse model of CIA. To create the experimental model of CIA, DAB-1 J male mice were injected with two doses of type II collagen subcutaneously into the base of the tail with a 22-day interval. The TIP3 treatment

schedule is outlined in Fig. 4a and described in the Methods section. To evaluate the relative therapeutic effect of TIP3 on RA, multiple parameters including body weight, paw volume, and the arthritis index were monitored over the treatment course. Between days 22 and 35, arthritic symptoms were clearly visible in all limbs, according to the images depicting swelling of the knee, ankle, and foot. By

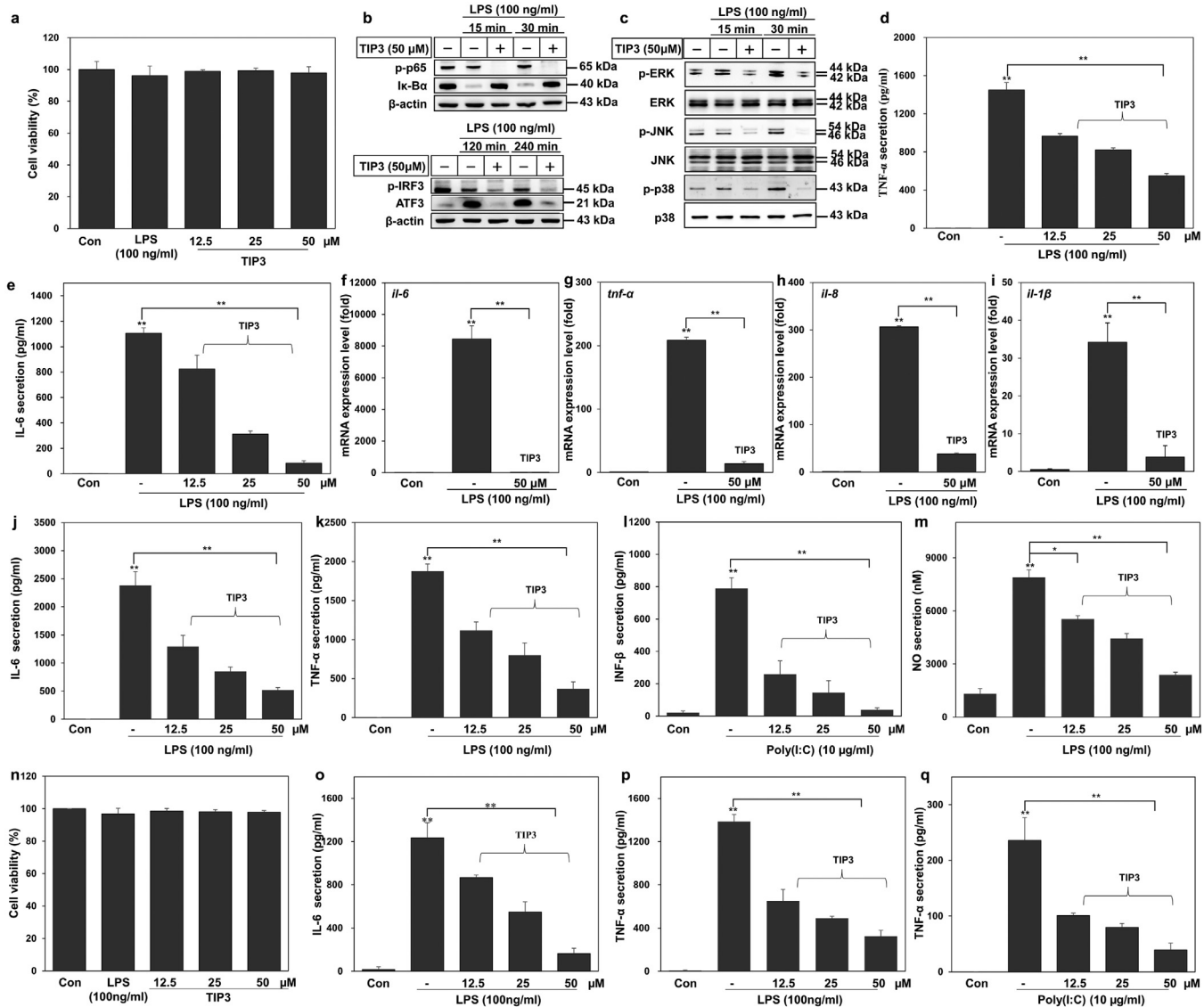


**Fig. 3.** Characterisation of the TLR-antagonistic effects of TIP3 on primary cells. (a) TIP3 was found to be safe for THP-1 cells at multiple concentrations ( $\leq 50 \mu\text{M}$ ) for 24 h. (b, c) The protein expression was measured by western blot analyses using hPBMCs. The amounts of p-p65, Iκ-Bα, p-IRF3, ATF3, p-ERK, ERK, p-JNK, JNK, p-p38 and p38 were evaluated in the total-protein extract. β-Actin served as a loading control. (d, e) The secretion levels of TNF-α and IL-6 were measured by ELISA after the cells were stimulated with LPS and then treated with TIP3. (f–i) The effects of TIP3 on the LPS-induced mRNA expression levels of IL-6, TNF-α, IL-8, and IL-1β after 4 h. The mRNA levels of these genes were substantially downregulated by TIP3. Values are indicated as fold changes (relative quantification; RQ) in mRNA levels, normalized to GAPDH. (j–m) The LPS-stimulated mbMDMs were treated with TIP3 for 1 h and the secretion levels of (j) IL-6 and (k) TNF-α were measured by an ELISA, and (m) the production of NO was evaluated using NO secretion kit. (l) The INF-β level was measured in poly(I:C)-stimulated mbMDMs through ELISA. (n–p) The LPS-stimulated hmNCs were also utilized to evaluate the secretion levels of (o) IL-6 and (p) TNF-α by ELISA. (q) The poly (I:C)-stimulated hmNCs were employed to assess the TLR3-inhibitory effect of TIP3 by measuring the TNF-α secretion by an ELISA. Effects similar to those of in RAW264.7 cells were detected. The data shown represent at least three independent experiments ( $n \geq 3$ ), and bars denote mean  $\pm$  SEM (\* $P < 0.05$ , \*\* $P < 0.01$ ) according to two-tailed Student's t-test.

contrast, the induction of RA was significantly attenuated in TIP3-injected mice as compared to CIA mice (Fig. 4b and Supp Fig. 2). During the entire period of arthritis development, the body weights of CIA mice decreased (average: 18.2 g), whereas those of normal (control) mice increased (average: 21.9 g). The loss of body weight was not observed in TIP3 (10 nmol/g)- and MTX-injected mice (average 20.5 and 21.0 g, respectively; Fig. 4c). The relative paw volume was measured in normal, CIA, and TIP3-injected mice. Compared to normal mice, the untreated CIA group had a large paw volume, but TIP3 (10 nmol/g)- and MTX-injected mice did not (Fig. 4d). The arthritis index also increased in the CIA mice, but TIP3 (10 nmol/g) or MTX treatment significantly decreased this index (Fig. 4e).

In the case of PAP-TIP3 (10 nmol/g)-treated mice (treatment started from day 35), the development of arthritis, indicated by paw volume and the arthritis index, was significantly inhibited when

compared with the CIA mice; however, we did not observe any significant change in body weight. To evaluate the extent of bone erosion reversal, we captured 3D images of knee joints and 2D images of trabecular and cortical bones of the normal, CIA, and TIP3 (10 nmol/g)-injected mice during *in vivo* micro-CT scanning (Supp Figs. 3–5). Severe erosion of bone and cartilage in the knee joint, loss of bone microarchitecture, depression of cortical thickness, and a reduction in bone mineral density were observed in the CIA mice compared with the normal mice (Fig. 4f–h). On the other hand, TIP3-treated mice experienced a remarkable recovery from the bone destruction and had a significantly lower inflammation score (Fig. 4f–j). Synovial hyperplasia, pannus formation, immune-cell infiltration, joint space narrowing, and thicker synovial tissues were clearly visible on histological examination of joint tissue sections stained with H&E in CIA mice. These symptoms were significantly reversed by the treatment

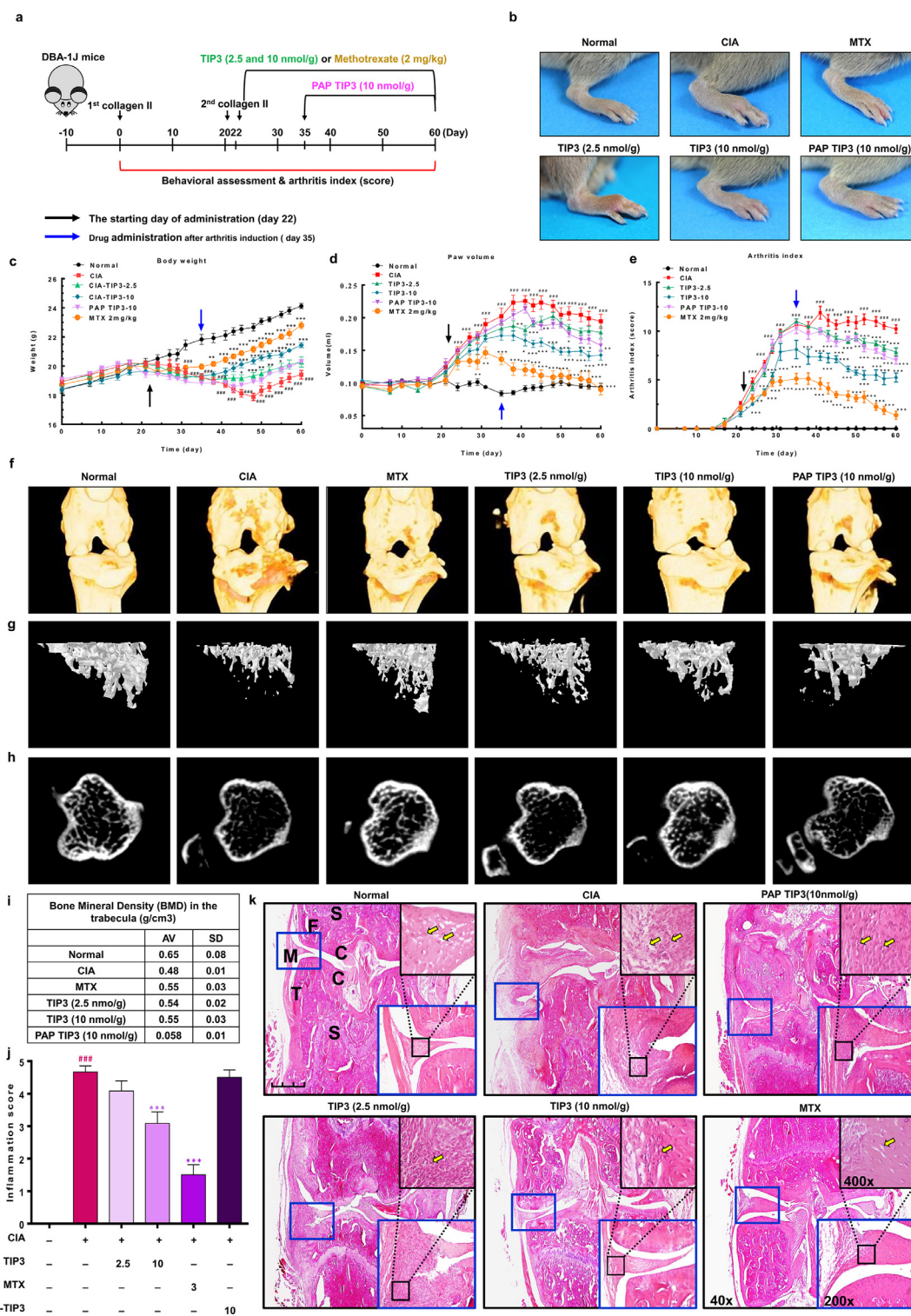


**Fig. 4.** The protective effect of TIP3 as evaluated in the mouse model of CIA by monitoring the anatomical and behavioural parameters. (a) An overview of the experimental protocol. The CIA was induced by subcutaneous injection of type II collagen into the mice. The TIP3 treatment was started either after the second injection of collagen (day 22) daily or after the postarthritis phase (PAP) (day 35) daily. Methotrexate served as a positive control. (b) The representative photographs of the paws were taken on day 45, and then magnified features of right hind paws were evaluated. (c–e) The mice were observed and analysed for their (c) body weight, (d) paw volume, and (e) arthritis index. The black and blue arrows indicate two time points of TIP3 treatment, as mentioned in (a). Numerical data are presented as mean  $\pm$  SEM:  $^{\#}P < 0.05$ ,  $^{##}P < 0.01$  and  $^{###}P < 0.001$  CIA versus Normal;  $*P < 0.05$ ,  $^{**}P < 0.01$  and  $^{***}P < 0.001$  TIP3 versus CIA. (f) The 3D images of the knee joints were captured by Micro-CT to estimate the joint corrosion and cartilage loss. (g) Representative 2D images of trabecular bone corresponding to the sagittal section at the top of the tibia and (h) cortical bone corresponding to the horizontal section in the middle of the tibia were captured by means of the micro-CT technology. (i) The bone mineral densities (BMDs) of the right or left knee joints were measured by Micro-CT, suggesting that TIP3 (10 nmol/g), similarly to MTX, restores mineral density. (j) The histogram representing quantification of the synovial hyperplasia score, suggesting that prolonged TIP3 treatment substantially reduces inflammation. (k) The histological evaluation of the CIA synovial tissues and the effect of TIP3 treatment. The images were taken at  $\times 40$  magnification, and the scale bar is 200  $\mu\text{m}$  in the normal case. The letters have the following meanings: C, cartilage; F, femur; M, meniscus; S, subchondral bone; T, tibia.

of the mice with 10 nmol/g TIP3, and this treatment effectively prevented these histopathological aberrations in a dose-dependent manner (Fig. 4k). These histological observations were in agreement with the above data from micro-CT images.

### 3.5. TIP3 exerts a significant therapeutic effect in the mouse model of psoriasis

Psoriasis is a chronic inflammatory skin disease characterised by amplified proliferation and altered differentiation of epidermis cells and inflammatory cell infiltrates [52]. Ample evidence implicates TLRs in the onset and progression of psoriasis [53–55]. Therefore, we decided to test the possible TIP3-mediated inhibition of TLRs and the underlying alleviation of symptoms in a psoriatic model. The disease was induced in 6–7-week-old C57BL/6 mice by the topical application of 62.5 mg of IMQ cream (5%) to their shaved back skin for 5 consecutive days (Fig. 5a). TIP3 was injected daily for 4 days at doses of 10 or 50 nmol/g, and the relevant consequences were evaluated. A reversal of inflammation severity was visible on the back skin of the TIP3-treated mice (Fig. 5b). Mice treated with 10 nmol/g TIP3 manifested a relatively weaker effect than did the MTX-treated group. Moreover, results on the PASI revealed that even though TIP3 did not significantly reduce the PASI score starting from day 2 (Fig. 5c), this peptide remarkably prevented splenomegaly in a dose-dependent manner (Fig. 5d). Treatment at a dose of 50 nmol/g had a much better effect, significantly decreasing the spleen weight (almost to the weight of normal murine spleen). The 50 nmol/g-treated group underwent a weight loss as compared to the MTX- and TIP3 (10 nmol/g)-treated groups (Fig. 5e). Furthermore, the histopathological changes and thickness of the skin in each group were evaluated by H&E staining; the data suggested that the treatment with both concentrations of TIP3 noticeably attenuated thickness of the epidermis (yellow arrowheads) and dermis (green arrowheads) in mice with the IMQ-induced psoriasis-like disease (Fig. 5f–h).

The hyperproliferative state of the skin and immune-cell infiltration (T cells or macrophages) are considered the major hallmarks of psoriasis. Hence, the effect of TIP3 on the skin infiltration by macrophages and Th17 cells was evaluated by immunohistochemical analysis of the back skin lesions in each group by means of primary antibodies recognizing CD68 (as a macrophage cell marker), CD4, or IL17 (as Th17 cell markers). The results showed that TIP3 effectively attenuated the overexpression of CD68, CD4, and IL-17 (brown staining) in mice with the IMQ-induced psoriasis-like disease, just as in the MTX-treated group (Fig. 5i and Supp Fig. 6).

### 3.6. The therapeutic effect of TIP3 on the mouse model of SLE

The therapeutic efficacy of TIP3 against systemic autoimmunity was evaluated next. MRL/lpr mutant mice were injected i.p. with a daily dose of 10 nmol/g TIP3 for 20 days (Fig. 6a). TIP3 significantly improved the health state of mice by reducing the lymphoid expansion and the spleen volume as compared to the vehicle-treated mice (Fig. 6b and c). Moreover, kidney inflammation can lead to a specific type of renal pathology known as glomerulonephritis. The latter is caused by SLE, and the evaluation of its severity could be done through the detection of particular circulating proteins such as albumin in urine. As depicted in Fig. 6d, urine content of albumin was reduced by TIP3 treatment. Furthermore, the production of dsDNA autoantibodies remained low after the treatment with TIP3 (Fig. 6e). A relatively low serum level of complement components, in particular C3 and C4, is a common marker of SLE. Accordingly, the C3 level was evaluated in the serum of TIP3-treated mice and was found to recover when compared to the mutant mice (Fig. 6f).

### 3.7. Biophysical and computational analysis revealed an interaction of TIP3 with the TLR TIR domain

A representative low-energy TIP3 model was docked with the TLR4 TIR domain to model the intermolecular interaction at the atomistic level (Fig. 7a). Because the BB loop of TLR TIR domains is a conserved element among TLR proteins (Supp Fig. 7) and is the site of adaptor recruitment [31], the binding site was anticipated around the BB loop residues for the docking calculation. TIP3 was predicted to dock onto the TIR domain with complementary surface geometry (Fig. 7b). A closer visual analysis suggested that amino acid residues K15 and D19 of TIP3 could form two hydrogen bonds with R689 and A720 (BB loop) of the TIR domain (Fig. 7c). Residues V22 and H24 of TIP3 are likely to establish hydrophobic interactions with V716 and I713 of the BB loop in the TIR domain. Because of the proximity between C23 of TIP3 and C664 of the TIR domain, an intermolecular disulphide bond could also be assumed. The TIP3 interacting residues on the TIR domain are highly conserved across different species (Supp Fig. 7a); however, these residues were largely variable across the TLR superfamily members (Supp Fig. 7b). Moreover, electrostatic potential surfaces on both molecules indicated that the BB loop region of the TIR domain comprises a dominant basic surface patch, while the TIP3 peptide (with two aspartates, D17 and D19) features a dominant acidic surface patch (Fig. 7e). This docking result and the electrostatic surface properties together suggest that TIP3 might have a potential affinity for the TIR domain. Furthermore, we conducted the SPR assay to confirm that TIP3 directly targets the TIR domain of TLR4 or TLR3. The result indicated that TIP3 binds to the TIR domains of TLR3 and TLR4 in a dose-dependent manner (Fig. 7f). Nevertheless, the relative binding kinetics of TIP3 toward these proteins could not be calculated from the available data. Advanced techniques such X-ray analysis are required for a better understanding of the TIP3 binding mechanism to TIR domains of these TLRs.

## 4. Discussion

Ligand-induced homo- and heterotypic TIR-TIR domain interactions are indispensable for the initiation of TLR signalling [56,57]. This highly compliant assembly of adaptor molecules has been proved crucial for the initiation of relevant signals, and blockage of these interfaces can abrogate TLR signalling [31]. Although, substantial efforts have been made to develop TLRs' ectodomain inhibitors, the cytoplasmic sites have been less explored. Because the adaptor molecules are involved in several overlapping pathways in a stoichiometric manner, relatively high potency and broader specificity may be anticipated from the inhibition of these proteins.

Dysregulated TLR signalling has been widely associated with the pathogenesis of autoimmune diseases, as stated above. Accordingly, many organic molecules and biologics have been tested in clinical trials to date [14,26]. Peptides may have better potency, selectivity, safety, and efficacy, which make them attractive candidates for future therapeutic strategies [58]. In a series of pioneering works, Toschakov et al. have reported peptide libraries mapped to the entire surface of TLR2, TLR4, or TLR9 TIR domains [31,59,60]. This decoy peptide approach has indicated the importance of BB loop-dependent intra/intermolecular TIR-TIR interactions between TLRs and/or adaptor proteins. Additionally, the surface exposed TIR peptides from TRIF, TRAM, and TIRAP have been explored to obtain effective TLR inhibitors [28,30,61]. These studies further confirm that not only the BB loop but also other segments, such as  $\alpha$ C and  $\alpha$ E helices as well as the AB loop of the TIR surface might play crucial roles in the initiation of TLR signalling. Likewise, another study has revealed that a TAT-conjugated TLR4 BB loop peptide (4BB) can reduce or reverse TLR4-dependent pain behaviour in rodents [62].

In the present study, we identified a potent TLR-inhibitory peptide (TIP3; derived from the first  $\beta$ -sheet [ $\beta$ A]) of TIRAP that successfully

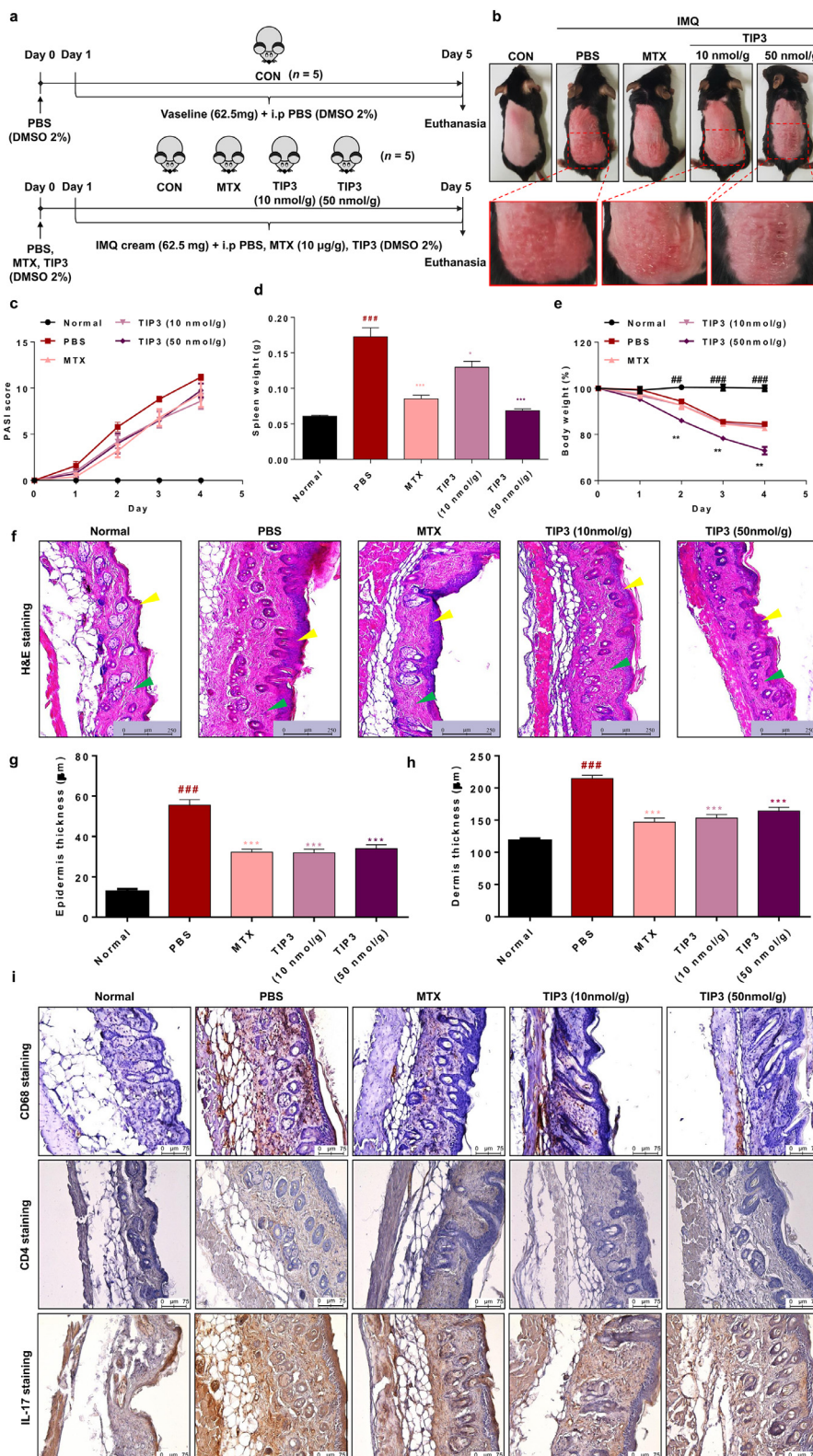


**Fig. 5.** The therapeutic efficacy of TIP3 in the mouse model of psoriasis. (a) The summarized experimental procedure for the therapeutic evaluation of TIP3 in the murine model of psoriasis. The disease was induced in C57BL/6 male mice by the topical application of imiquimod (IMQ). TIP3 was administered i.p. before the IMQ application. Methotrexate (MTX) served as a positive control for the relative therapeutic evaluation of TIP3. (b) Photographs of back skin on day 4, indicating the therapeutic effect of TIP3 relative to the untreated and MTX treated groups. (c) Scoring of disease severity based on the clinical Psoriasis Area and Severity Index (PASI). Light and dark purple lines indicate the PASI score of mice treated with TIP3 at 10 and 50 nmol/g, respectively. (d) The influence of TIP3 on spleen weight. (e) Body weight dynamics of mice during the treatment regimen. (f) The effect of TIP3 on the thickness of the epidermis (yellow arrowheads) and dermis (green arrowheads). (g, h) The thickness of the skin in each group was measured with the Leica DMi8 fluorescence microscope. (i) Immunohistochemical analysis of the back skin lesions in each group. The scale bar is 75  $\mu$ m for high-magnification images. Data represent mean  $\pm$  SEM from five skin tissue samples from each group. \*\*\* $P < 0.001$  between NC and PBS, \* $P < 0.05$ , \*\* $P < 0.01$  between PBS and TIP3 at 10 or 50 nmol or MTX, according to two-tailed Student's t-test.

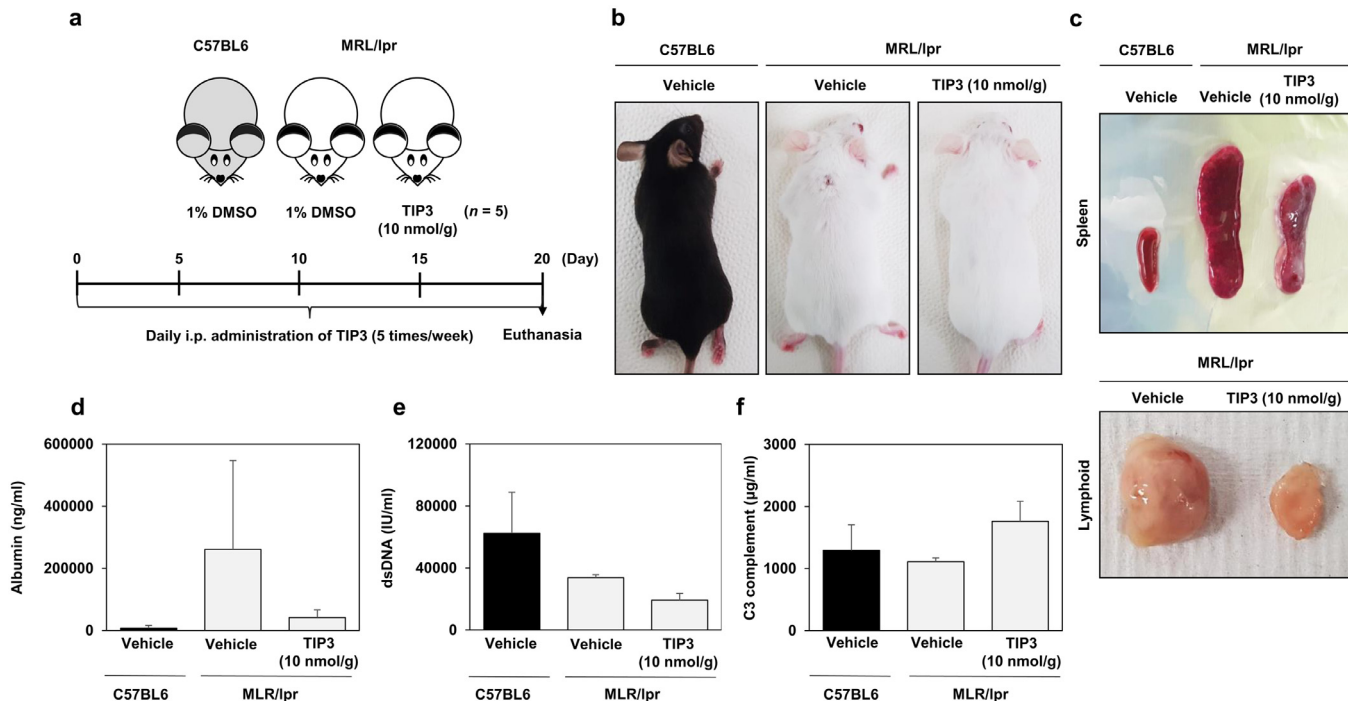


**Fig. 6.** The promising inhibitory effect of TIP3 on SLE in a mouse model. (a) A summary of the experimental validation of the inhibitory effect of TIP3 on SLE in the mouse model. (b) C57BL6 male mice and lupus-prone mice are shown in the images. (c) The ameliorative effect of TIP3 on lymphoproliferation according to photographs of the spleen and lymph nodes. (d) Albumin content of urine, (e) concentration of anti-dsDNA antibodies, and (f) of the C3 complement component in serum were determined by ELISA. The exact Wilcoxon Rank Sum test (which is numerically equivalent to the Mann–Whitney U test) was performed to compare the mean values between the two groups. \* $P < 0.05$  and \*\* $P < 0.01$ .

reduces the TLR4-mediated secretion of proinflammatory cytokines. Initially, the TLR4-inhibitory effect was confirmed by evaluating the LPS-induced NF- $\kappa$ B activation in HEK-Blue™ hTLR4 cells. Because TLR4 conveys the immune signalling through both the MyD88 and TRIF adaptor molecules, we decided to determine whether TIP3 blocks both arms of TLR4 signalling. TIP3 inhibited both the LPS-induced proinflammatory cytokine and type I interferon induction in the murine and human macrophages (Figs. 2 and 3), suggesting that TIP3 is capable of inhibiting both MyD88- and TRIF-dependent signalling. Furthermore, TIP3 was evaluated for broad-range TLRs inhibition by measuring the TNF- $\alpha$  secretion from RAW264.7 cells activated by different TLR ligands. We found that TNF- $\alpha$  secretion that is dependent on TLR4 and TLR3, but not on other TLRs, was substantially inhibited by TIP3 (Fig. 2e, m, and n). The negligible inhibitory effect of TIP3 on TLR2-, 7-, 8-, and 9-mediated signalling pathways could be due to the variation in the TIP3-binding interface on their TIR domains. The ELISA results were then confirmed by the western blot analysis and followed by mRNA quantification of the multiple transcription factors and proinflammatory cytokines, in various established and primary human and mouse cell lines.

Ample evidence implicates TLRs in the pathogenesis of autoimmune diseases [63–65]. The involvement of TLR4 in the onset of chronic destructive arthritis has been previously investigated in murine models of CIA and of IL-1Ra-deficient ( $IL-1Ra^{-/-}$ ) arthritis; this research has uncovered remarkable alleviation of the clinical and histological manifestations of the disease [66]. Besides, several studies have identified the abundance of endogenous TLR4 ligands such as HSPs,  $\alpha$ A-crystallin, HSPB8 [67], and tenascin C [68,69] and significantly elevated concentrations of high-mobility group box 1 in the synovial fluid of patients with RA [70,71]. Furthermore, in RA patients, the expression of both TLR4 and TLR3 was reported to be significantly higher when compared with healthy individuals [20,21].

Overall, the implication of TLRs in the development and progression of RA make them promising therapeutic targets. Consequently, we tested the protective effect of TIP3 against RA in a murine CIA

model. TIP3 significantly attenuated the induction of RA, reversed the body weight loss, decreased the paw volume, and decreased the arthritis index in the CIA mice. The peptide partially promoted the reversal of the bone and cartilage erosion by promoting a regain of bone microarchitecture and mineral composition regain (Fig. 4). Moreover, TIP3 attenuated the histopathological aberrations by reducing the intensive immune-cell infiltration, by decreasing the thickness of synovial tissues, and by recovering normal spacing within the joint.

The therapeutic effect of TIP3 was further investigated in animal models of psoriasis and lupus. TIP3 significantly ameliorated the skin lesions, prevented splenomegaly, and improved the overall physiological state of these mice. TIP3 also ameliorated the histological symptoms of the disease by attenuating the increase in epidermis and dermis thickness and by inhibiting the hyperproliferative state of the skin. Despite the dose-dependent protective effect of the peptide, a noticeable weight loss was observed at the 50 nmol/g dose of TIP3. Nonetheless, this problem may not be solely due to the peptide treatment because we observed a significant weight recovery in the CIA model when treated at 10 nmol/g (Fig. 4c). TIP3 also prevented the lymphoproliferation in the mouse model of SLE and downregulated glomerulonephritis markers by reducing the concentration of albumin in urine. Besides, the production of anti-dsDNA autoantibodies was reduced by the TIP3 treatment, while the levels of complement components C4 and C3 were recovered.

Numerous investigators have suggested that the TIR domains in the TLR family share a high degree of structural similarity and belong to one of the most evolutionarily conserved families of structural folds, which are also found in bacteria [72] and plants [73]. In particular, the BB loop and its adjacent regions are believed to be highly conserved, which represent principal locations for TIR dimerisation and are the site of adaptor recruitment [74]. Our computational docking simulations revealed that TIP3 has suitable surface geometry and electrostatic surface properties for binding to the TLR4 TIR domain. The intermolecular interactions were stabilized by both nonpolar

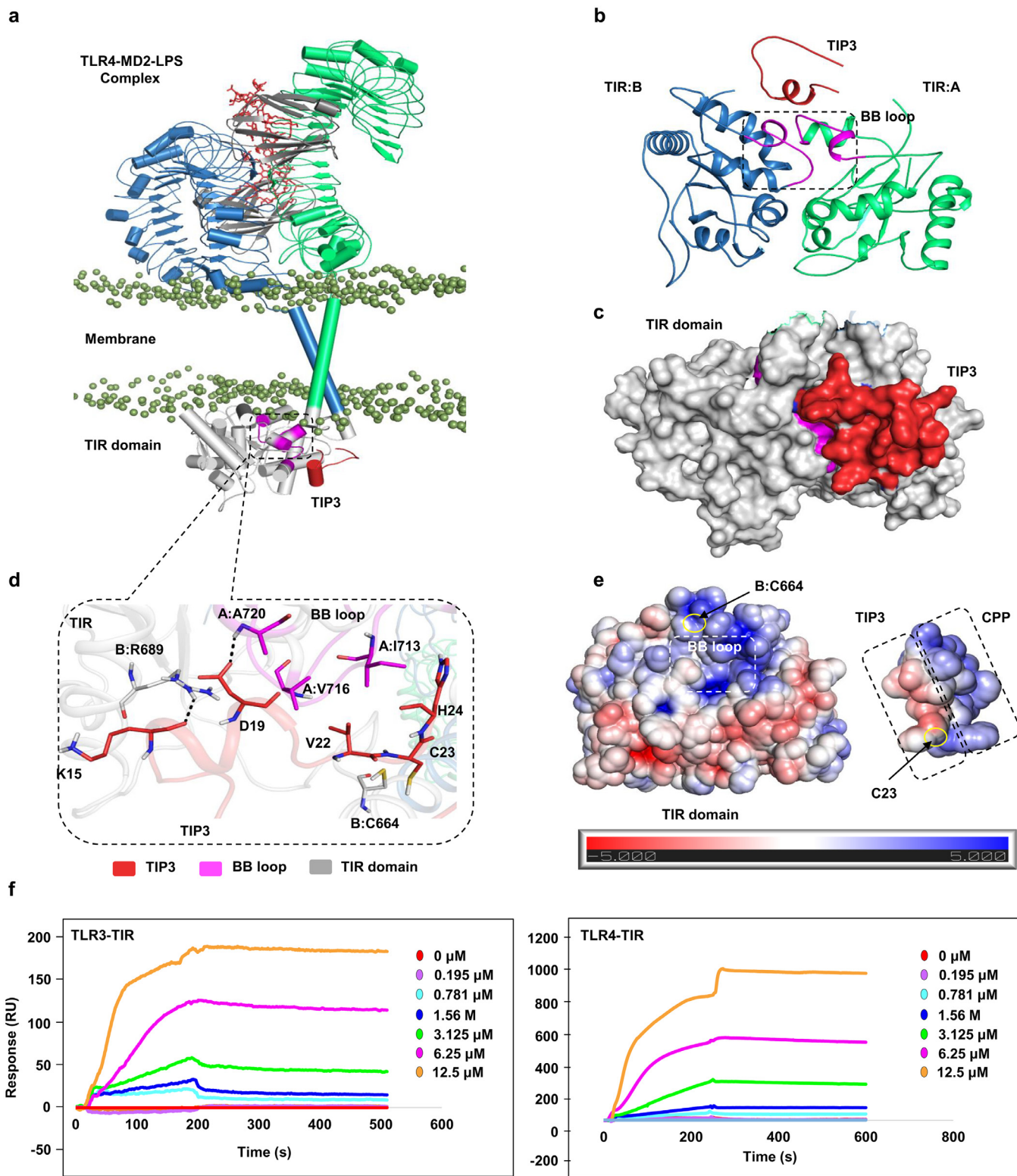


**Fig. 7.** Detailed intermolecular interaction between TIP3 and the TIR domain of TLR4. (a) The overall docked model of TIP3 (red cartoon) with the full-length TLR4 model. Chains A and B of TLR4 are coloured green and blue, respectively. The TLR4 coreceptor, myeloid differentiation factor-2 (MD2), is coloured grey, and LPS is displayed as a red stick model. Phosphate groups (mauve beads) of the phospholipid bilayer are used to indicate the membrane region. The TIR domains are presented as a grey space-fill model, and the BB loop is magenta. (b) A representative docked pose of TIP3 on the TLR4 TIR domain, extracted from panel (a), showing the binding of the peptide to the BB loop surface of the TIR domain. (c) Surface view of TIP3 (red) bound to the TIR domain (grey) of TLR4. (d) Detailed view of the interaction between TIP3 residues with those of the TLR4 TIR domain. TIP3 residues are red, TIR residues are grey, and BB loop residues are magenta. Residues of the B chain of TLR4 are indicated by "B" followed by the residue number. (e) The electrostatic potential surface of the TLR4 TIR domain and TIP3 peptide. The BB loop region of the TIR domain, the CPP, and the bioactive segment of TIP3 peptide are indicated with dashed boxes. C664 of the TIR domain and C23 of TIP3, which may form an intermolecular disulphide bridge, are marked with a yellow circle. (f) The sensorgram of the potential binding of TIP3 to the TIR domains of TLR3 and TLR4.

and electrostatic interactions along with hydrogen bonds involving main-chain atoms. TIP3 penetrates the cell membrane and inhibits the MyD88-dependent as well as -independent pathways by possibly binding to the adaptor docking sites in the TLR TIR domains. For this reason, in the absence of the experimental structure of a given TIR domain, homology modelling has been widely employed to construct a 3D model based on plausible hypotheses about the homodimerisation, receptor binding, and adaptor-binding interfaces [75–78]. Several important hypothesis-driven studies on TLR TIR domains have been conducted on homology models of TIR domains based on the X-ray crystallographic structure of the TLR10 TIR domain [31,77,79]. Recently, a 7-A-resolution cryo-electron-microscopic structure of TIRAP was reported [73], where two parallel strands of TIR domains are arranged in a BB-loop mediated head-to-tail manner. Although the large filamentous arrangement of TIRAP or MyD88 TIR domains is unlikely to form during cellular signalling, the importance of BB loops in TIR-TIR interaction has certainly been elucidated. These findings indicate that any disturbance of the BB loop surface may break the dimeric association of TIR domains and/or disrupt their association with the TLR proteins. In light of this and other concurrent evidence, TIP3 is likely to target the TLR TIR domain and will serve not only as a valuable probe for better elucidation of the TLR signalling pathways but also as a lead candidate in terms of TLR-targeting therapeutics.

### Declaration of competing interest

The authors declare that there are no conflicts of interest.

### Supplementary materials

Supplementary material associated with this article can be found in the online version at doi:[10.1016/j.ebiom.2020.102645](https://doi.org/10.1016/j.ebiom.2020.102645).

### References

- [1] Kawai T, Akira S. The role of pattern-recognition receptors in innate immunity: update on Toll-like receptors. *Nat Immunol* 2010;11(5):373–84.
- [2] Gay NJ, Gangloff M, Weber AN. Toll-like receptors as molecular switches. *Nat Rev Immunol* 2006;6(9):693–8.
- [3] O'Neill LA, Bowie AG. The family of five: tIR-domain-containing adaptors in Toll-like receptor signalling. *Nat Rev Immunol* 2007;7(5):353–64.
- [4] Gay NJ, Symmons MF, Gangloff M, Bryant CE. Assembly and localization of Toll-like receptor signalling complexes. *Nat Rev Immunol* 2014;14(8):546–58.
- [5] Lin SC, Lo YC, Wu H. Helical assembly in the MYD88-IRAK4-IRAK2 complex in TLR/IL-1R signalling. *Nature* 2010;465(7300):885–90.
- [6] Gay NJ, Gangloff M, O'Neill LA. What the Myddosome structure tells us about the initiation of innate immunity. *Trends Immunol* 2011;32(3):104–9.
- [7] Iwasaki A, Medzhitov R. Control of adaptive immunity by the innate immune system. *Nat Immunol* 2015;16(4):343–53.
- [8] Wu YW, Tang W, Zuo JP. Toll-like receptors: potential targets for lupus treatment. *Acta Pharmacol Sin* 2015;36(12):1395–407.
- [9] Wang Y, Chen L, Li F, et al. TLR4 rs41426344 increases susceptibility of rheumatoid arthritis (RA) and juvenile idiopathic arthritis (JIA) in a central south Chinese Han population. *Pediatr Rheumatol Online J* 2017;15(1):12.
- [10] Jimenez-Dalmaroni MJ, Gerswhin ME, Adamopoulos IE. The critical role of toll-like receptors—From microbial recognition to autoimmunity: a comprehensive review. *Autoimmun Rev* 2016;15(1):1–8.
- [11] Feldman N, Rotter-Maskowtiz A, Okun E. DAMPs as mediators of sterile inflammation in aging-related pathologies. *Ageing Res Rev* 2015;24(Pt A):29–39.
- [12] Liew FY, Xu D, Brint EK, O'Neill LA. Negative regulation of toll-like receptor-mediated immune responses. *Nat Rev Immunol* 2005;5(6):446–58.
- [13] O'Neill LA, Bryant CE, Doyle SL. Therapeutic targeting of Toll-like receptors for infectious and inflammatory diseases and cancer. *Pharmacol Rev* 2009;61(2):177–97.
- [14] Ache A, Yesudhas D, Choi S. Toll-like receptors: promising therapeutic targets for inflammatory diseases. *Arch Pharm Res* 2016;39(8):1032–49.
- [15] Yesudhas D, Gosu V, Anwar MA, Choi S. Multiple roles of toll-like receptor 4 in colorectal cancer. *Front Immunol* 2014;5:334.
- [16] Gomez R, Villalvilla A, Largo R, Gualillo O, Herrero-Beaumont G. TLR4 signalling in osteoarthritis—finding targets for candidate DMOADs. *Nat Rev Rheumatol* 2015;11(3):159–70.
- [17] Joosten LA, Abdollahi-Roodsaz S, Dinarello CA, O'Neill L, Netea MG. Toll-like receptors and chronic inflammation in rheumatic diseases: new developments. *Nat Rev Rheumatol* 2016;12(6):344–57.
- [18] Marshak-Rothstein A. Toll-like receptors in systemic autoimmune disease. *Nat Rev Immunol* 2006;6(11):823–35.
- [19] Guo H, Callaway JB, Ting JP. Inflammasomes: mechanism of action, role in disease, and therapeutics. *Nat Med* 2015;21(7):677–87.
- [20] Ospeit C, Brentano F, Rengel Y, et al. Overexpression of toll-like receptors 3 and 4 in synovial tissue from patients with early rheumatoid arthritis: toll-like receptor expression in early and longstanding arthritis. *Arthritis Rheum* 2008;58(12):3684–92.
- [21] Kowalski ML, Wolska A, Grzegorczyk J, et al. Increased responsiveness to toll-like receptor 4 stimulation in peripheral blood mononuclear cells from patients with recent onset rheumatoid arthritis. *Mediators Inflamm* 2008;2008:132732.
- [22] Liu B, Yang Y, Dai J, et al. TLR4 up-regulation at protein or gene level is pathogenic for lupus-like autoimmune disease. *J Immunol* 2006;177(10):6880–8.
- [23] Reynolds JM, Martinez GJ, Chung Y, Dong C. Toll-like receptor 4 signalling in T cells promotes autoimmune inflammation. *Proc Natl Acad Sci USA* 2012;109(32):13064–9.
- [24] Patra MC, Shah M, Choi S. Toll-like receptor-induced cytokines as immunotherapeutic targets in cancers and autoimmune diseases. *Semin Cancer Biol* 2020 In press. doi: [10.1016/j.semancer.2019.05.002](https://doi.org/10.1016/j.semancer.2019.05.002).
- [25] Zuany-Amorim C, Hastewell J, Walker C. Toll-like receptors as potential therapeutic targets for multiple diseases. *Nat Rev Drug Discov* 2002;1(10):797–807.
- [26] Hennessy EJ, Parker AE, O'Neill LA. Targeting Toll-like receptors: emerging therapeutics? *Nat Rev Drug Discov* 2010;9(4):293–307.
- [27] O'Neill LA. Therapeutic targeting of Toll-like receptors for inflammatory and infectious diseases. *Curr Opin Pharmacol* 2003;3(4):396–403.
- [28] Couture LA, Piao W, Ru LW, Vogel SN, Toshchakov VY. Targeting Toll-like receptor (TLR) signalling by Toll/interleukin-1 receptor (TIR) domain-containing adapter protein/MyD88 adapter-like (TIRAP/Mal)-derived decoy peptides. *J Biol Chem* 2012;287(29):24641–8.
- [29] Park S, Shin HJ, Shah M, et al. TLR4/MD2 specific peptides stalled *in vivo* LPS-induced immune exacerbation. *Biomaterials* 2017;126:49–60.
- [30] Piao W, Vogel SN, Toshchakov VY. Inhibition of TLR4 signaling by TRAM-derived decoy peptides *in vitro* and *in vivo*. *J Immunol* 2013;190(5):2263–72.
- [31] Toshchakov VY, Szmacinski H, Couture LA, Lakowicz JR, Vogel SN. Targeting TLR4 signaling by TLR4 Toll/IL-1 receptor domain-derived decoy peptides: identification of the TLR4 Toll/IL-1 receptor domain dimerization interface. *J Immunol* 2011;186(8):4819–27.
- [32] Piao W, Shirey KA, Ru LW, et al. A decoy peptide that disrupts tirap recruitment to TLRs is protective in a murine model of influenza. *Cell Rep* 2015;11(12):1941–52.
- [33] Bonham KS, Orzalli MH, Hayashi K, et al. A promiscuous lipid-binding protein diversifies the subcellular sites of toll-like receptor signal transduction. *Cell* 2014;156(4):705–16.
- [34] Kagan JC, Medzhitov R. Phosphoinositide-mediated adaptor recruitment controls Toll-like receptor signalling. *Cell* 2006;125(5):943–55.
- [35] Hughes MM, Lavrencic P, Coll RC, et al. Solution structure of the TLR adaptor MAL/TIRAP reveals an intact BB loop and supports MAL CYS91 glutathionylation for signaling. *Proc Natl Acad Sci USA* 2017;114(32):E6480–E9.
- [36] Lin Z, Lu J, Zhou W, Shen Y. Structural insights into TIR domain specificity of the bridging adaptor MAL in TLR4 signaling. *PLoS ONE* 2012;7(4):e34202.
- [37] Valkov E, Stamp A, Dimaio F, et al. Crystal structure of Toll-like receptor adaptor MAL/TIRAP reveals the molecular basis for signal transduction and disease protection. *Proc Natl Acad Sci USA* 2011;108(36):14879–84.
- [38] Zhao X, Xiong W, Xiao S, et al. Membrane targeting of TIRAP is negatively regulated by phosphorylation in its phosphoinositide-binding motif. *Sci Rep* 2017;7:43043.
- [39] Kwon HK, Shin HJ, Lee JH, et al. Etoposide induces necrosis through p53-Mediated antiapoptosis in human kidney proximal tubule cells. *Toxicol Sci: an official journal of the Society of Toxicology* 2015;148(1):204–19.
- [40] Kwon HK, Lee JH, Shin HJ, Kim JH, Choi S. Structural and functional analysis of cell adhesion and nuclear envelope nano-topography in cell death. *Sci Rep* 2015;5:15623.
- [41] Xin W, Huang C, Zhang X, et al. Methyl salicylate lactoside inhibits inflammatory response of fibroblast-like synoviocytes and joint destruction in collagen-induced arthritis in mice. *Br J Pharmacol* 2014;171(14):3526–38.
- [42] Bang JS, Oh DH, Choi HM, et al. Anti-inflammatory and antiarthritic effects of pipericine in human interleukin 1beta-stimulated fibroblast-like synoviocytes and in rat arthritis models. *Arthritis Res Ther* 2009;11(2):R49.
- [43] Kim BH, Kim M, Yin CH, et al. Inhibition of the signalling kinase JAK3 alleviates inflammation in monoarthritic rats. *Br J Pharmacol* 2011;164(1):106–18.
- [44] Kwon HK, Patra MC, Shin HJ, et al. A cell-penetrating peptide blocks toll-like receptor-mediated downstream signaling and ameliorates autoimmune and inflammatory diseases in mice. *Exp Mol Med* 2019;51(4):50.
- [45] Derossi D, Joliot AH, Chassaing G, Prochiantz A. The third helix of the antennapedia homeodomain translocates through biological membranes. *J Biol Chem* 1994;269(14):10444–50.
- [46] Akira S, Takeda K. Toll-like receptor signalling. *Nat Rev Immunol* 2004;4(7):499–511.
- [47] Schett G, Dayer JM, Manger B. Interleukin-1 function and role in rheumatic disease. *Nat Rev Rheumatol* 2016;12(1):14–24.
- [48] Kim JY, Park SJ, Yun KJ, Cho YW, Park HJ, Lee KT. Isoliquiritigenin isolated from the roots of Glycyrrhiza uralensis inhibits LPS-induced iNOS and COX-2 expression via the attenuation of NF-KAPPAB in raw 264.7 macrophages. *Eur J Pharmacol* 2008;584(1):175–84.
- [49] Yang CS, Lee DS, Song CH, et al. Roles of peroxiredoxin II in the regulation of proinflammatory responses to LPS and protection against endotoxin-induced lethal shock. *J Exp Med* 2007;204(3):583–94.
- [50] West AP, Brodsky IE, Rahner C, et al. TLR signalling augments macrophage bactericidal activity through mitochondrial ROS. *Nature* 2011;472(7344):476–80.

- [51] Roelofs MF, Wenink MH, Brentano F, et al. Type I interferons might form the link between Toll-like receptor (TLR) 3/7 and TLR4-mediated synovial inflammation in rheumatoid arthritis (RA). *Ann Rheum Dis* 2009;68(9):1486–93.
- [52] Schon MP, Boehncke WH, Brocker EB. Psoriasis: clinical manifestations, pathogenesis and therapeutic perspectives. *Discov Med* 2005;5(27):253–8.
- [53] Baker BS, Ovigne JM, Powles AV, Corcoran S, Fry L. Normal keratinocytes express Toll-like receptors (TLRs) 1, 2 and 5: modulation of TLR expression in chronic plaque psoriasis. *Br J Dermatol* 2003;148(4):670–9.
- [54] Begon E, Michel L, Flageul B, et al. Expression, subcellular localization and cytosolic modulation of Toll-like receptors (TLRs) in normal human keratinocytes: TLR2 up-regulation in psoriatic skin. *Eur J Dermatol EJD* 2007;17(6):497–506.
- [55] Hirai T, Kanda T, Sato K, et al. Cathepsin K is involved in development of psoriasis-like skin lesions through TLR-dependent Th17 activation. *J Immunol* 2013;190(9):4805–11.
- [56] Vyncke L, Bovijn C, Pauwels E, et al. Reconstructing the TIR side of the myddosome: a paradigm for tir-tir interactions. *Structure* 2016;24(3):437–47.
- [57] Bovijn C, Desmet AS, Uyttendaele I, Van Acker T, Tavernier J, Peelman F. Identification of binding sites for myeloid differentiation primary response gene 88 (MyD88) and Toll-like receptor 4 in MYD88 adapter-like (Mal). *J Biol Chem* 2013;288(17):12054–66.
- [58] Fosgerau K, Hoffmann T. Peptide therapeutics: current status and future directions. *Drug Discov Today* 2015;20(1):122–8.
- [59] Javmen A, Szmacinski H, Lakowicz JR, Toshchakov VY. Blocking TIR domain interactions in TLR9 signaling. *J Immunol* 2018;201(3):995–1006.
- [60] Toshchakov VY, Fenton MJ, Vogel SN. Cutting edge: differential inhibition of TLR signaling pathways by cell-permeable peptides representing BB loops of TLRs. *J Immunol* 2007;178(5):2655–60.
- [61] Piao W, Ru LW, Piepenbrink KH, Sundberg EJ, Vogel SN, Toshchakov VY. Recruitment of tlr adapter trif to TLR4 signaling complex is mediated by the second helical region of TRIF/TIR domain. *Proc Natl Acad Sci USA* 2013;110(47):19036–41.
- [62] Allette YM, Kim Y, Randolph AL, Smith JA, Ripsch MS, White FA. Decoy peptide targeted to Toll-IL-1R domain inhibits LPS and TLR4-active metabolite morphine-3 glucuronide sensitization of sensory neurons. *Sci Rep* 2017;7(1):3741.
- [63] Liu Y, Yin H, Zhao M, Lu Q. TLR2 and TLR4 in autoimmune diseases: a comprehensive review. *Clin Rev Allergy Immunol* 2014;47(2):136–47.
- [64] Smith RL, Hebert HL, Massey J, et al. Association of Toll-like receptor 4 (TLR4) with chronic plaque type psoriasis and psoriatic arthritis. *Arch Dermatol Res* 2016;308(3):201–5.
- [65] Lartigue A, Colliou N, Calbo S, et al. Critical role of TLR2 and TLR4 in autoantibody production and glomerulonephritis in lpr mutation-induced mouse lupus. *J Immunol* 2009;183(10):6207–16.
- [66] Abdollahi-Roodsaz S, Joosten LA, Roelofs MF, et al. Inhibition of Toll-like receptor 4 breaks the inflammatory loop in autoimmune destructive arthritis. *Arthritis Rheum* 2007;56(9):2957–67.
- [67] Roelofs MF, Boelens WC, Joosten LA, et al. Identification of small heat shock protein B8 (HSP22) as a novel TLR4 ligand and potential involvement in the pathogenesis of rheumatoid arthritis. *J Immunol* 2006;176(11):7021–7.
- [68] Midwood KS, Orend G. The role of tenascin-C in tissue injury and tumorigenesis. *J Cell Commun Signal* 2009;3(3–4):287–310.
- [69] Page TH, Charles PJ, Piccinini AM, Nicolaidou V, Taylor PC, Midwood KS. Raised circulating tenascin-C in rheumatoid arthritis. *Arthritis Res Ther* 2012;14(6):R260.
- [70] Park SY, Lee SW, Kim HY, Lee WS, Hong KW, Kim CD. HMGB1 induces angiogenesis in rheumatoid arthritis via HIF-1alpha activation. *Eur J Immunol* 2015;45(4):1216–27.
- [71] Taniguchi N, Kawahara K, Yone K, et al. High mobility group box chromosomal protein 1 plays a role in the pathogenesis of rheumatoid arthritis as a novel cytokine. *Arthritis Rheum* 2003;48(4):971–81.
- [72] Alaidarus M, Ve T, Casey LW, et al. Mechanism of bacterial interference with TLR4 signaling by Brucella Toll/interleukin-1 receptor domain-containing protein TCPB. *J Biol Chem* 2014;289(2):654–68.
- [73] Zhang X, Bernoux M, Bentham AR, et al. Multiple functional self-association interfaces in plant TIR domains. *Proc Natl Acad Sci USA* 2017;114(10):E2046–E52.
- [74] Dunne A, O'Neill LA. The interleukin-1 receptor/Toll-like receptor superfamily: signal transduction during inflammation and host defense. *Sci STKE*: Signal Transduct Knowl Environ 2003;2003(171):re3.
- [75] Gautam JK, Ashish, Comeau LD, Krueger JK, Smith Jr. MF. Structural and functional evidence for the role of the TLR2 DD loop in TLR1/TLR2 heterodimerization and signaling. *J Biol Chem* 2006;281(40):30132–42.
- [76] Jiang Z, Georgel P, Li C, et al. Details of toll-like receptor:adapter interaction revealed by germ-line mutagenesis. *Proc Natl Acad Sci USA* 2006;103(29):10961–6.
- [77] Dunne A, Ejdeback M, Ludidi PL, O'Neill LA, Gay NJ. Structural complementarity of Toll/Interleukin-1 receptor domains in Toll-like receptors and the adaptors MAL and MYD88. *J Biol Chem* 2003;278(42):41443–51.
- [78] Li C, Zienkiewicz J, Hawiger J. Interactive sites in the MYD88 Toll/Interleukin (IL) 1 receptor domain responsible for coupling to the IL1beta signaling pathway. *J Biol Chem* 2005;280(28):26152–9.
- [79] Nunez Miguel R, Wong J, Westoll JF, et al. A dimer of the Toll-like receptor 4 cytoplasmic domain provides a specific scaffold for the recruitment of signalling adaptor proteins. *PLoS ONE* 2007;2(8):e788.